AD-A083 038 UTAH STATE UNIV LOGAN CENTER FOR ATMOSPHERIC AND SPA--ETC F/G 4/1
ENERGY INPUT TO THE AURORAL IONOSPHERE.(U)
FEB 80 J R DOUPNIK
AFOSR-77-3435
UNCLASSIFIED AFOSR-TR-80-0261 NL

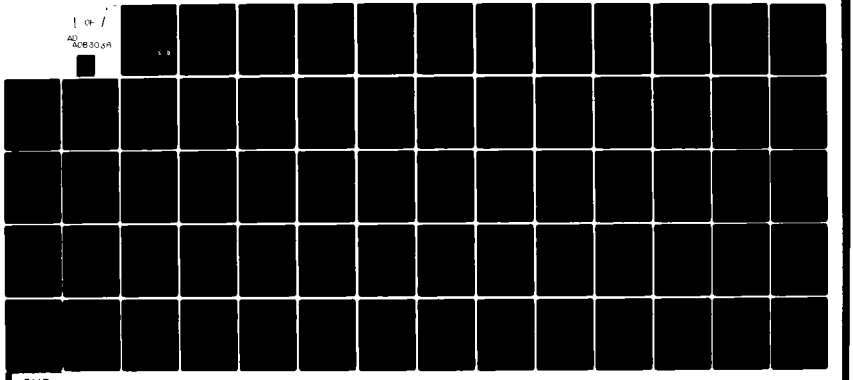

END
DATE FILMED
5-80
DTIC

SECURITY CLASSIFICATION OF THIS PAGE (When Data Entered) Unclassified

LEVEL II

REPORT DOCUMENTATION PAGE

READ INSTRUCTIONS BEFORE COMPLETING FORM

1. REPORT NUMBER: AFOSR-TR-80-0261	2. GOVT ACCESSION NO.
3. RECIPIENT'S CATALOG NUMBER	
4. TITLE (and Subtitle): Energy Input to the Auroral Ionosphere,	5. TYPE OF REPORT & PERIOD COVERED: Final Report, 1 Sep 77 — 31 Aug 78
6. PERFORMING ORG. REPORT NUMBER	
7. AUTHOR(s): J. R. Doupnik	8. CONTRACT OR GRANT NUMBER(s): AFOSR-77-3435
9. PERFORMING ORGANIZATION NAME AND ADDRESS: Utah State University, Center for Atmospheric and Space Sciences, Logan, Utah 84322	10. PROGRAM ELEMENT, PROJECT, TASK AREA & WORK UNIT NUMBERS: 61102F, 2310/A2
11. CONTROLLING OFFICE NAME AND ADDRESS: AF Office of Scientific Research/NC, Bldg. 410, Bolling AFB, DC 20332	12. REPORT DATE: 29 February 1980
	13. NUMBER OF PAGES: 66
14. MONITORING AGENCY NAME & ADDRESS (if different from Controlling Office)	15. SECURITY CLASS. (of this report): Unclassified
	15a. DECLASSIFICATION/DOWNGRADING SCHEDULE

AD A083038

16. DISTRIBUTION STATEMENT (of this Report)

Approved for public release; distribution unlimited.

17. DISTRIBUTION STATEMENT (of the abstract entered in Block 20, if different from Report)

DTIC ELECTE S APR 11 1980 D B

18. SUPPLEMENTARY NOTES

19. KEY WORDS (Continue on reverse side if necessary and identify by block number)

Ionosphere	Millstone Hill
Joule Heating	Auroral Oval
Chatanika Radar	Plasma Flow

20. ABSTRACT (Continue on reverse side if necessary and identify by block number)

This effort was to aid studies of the high latitude ionosphere particularly with regard to Joule heating processes. For energy input to the atmosphere by Joule heating the dominant physical factor has been found to be the strength of the electric field - the motions of the ionospheric plasma through the nearly stationary neutral gas. Both the conductivity and electric field change by large factors but the dependence of the Joule heating rate on the square of the electric field strength makes the electric field the most critical factor. In

DD FORM 1 JAN 73 1473

UNCLASSIFIED

SECURITY CLASSIFICATION OF THIS PAGE (When Data Entered)

DTIC FILE COPY

Item 9. (cont)

the design of the experiments with a steerable dish antenna the conductivities are obtained from electron densities in the E region of the ionosphere while the electric fields are obtained from the F region. In this work, to cover a wide range of latitudes with acceptable time resolution, the E region measurements were curtailed. Two series of experiments were conducted with the Chatanika radar in Alaska; one in January 1978 and the second in June 1978. An objective of the June series was to study the global pattern versus temporal fluctuation by simultaneously operating the Millstone Hill radar located in Massachusetts. An exploratory trip to Millstone Hill was made in May 1978 to learn how that system functioned. The raw radar data were recorded on tape and processed on the CASS Computer Facility computer to give geophysical parameters of plasma densities and drift velocities. A finding from these and subsequent similar experiments is that the electric field pattern (strength and direction) is surprisingly smooth over large ranges of latitudes and over long periods of local time. The local afternoon sector (22 hours UT is local noon at Chatanika) is characterized by very strong electric fields which increase rapidly with latitude. Small changes in the diameter of the auroral oval due to substorms or fluctuations in the solar wind produce large variations of the field strength over Chatanika without necessarily altering the overall electric field pattern. This means the Joule heating during the afternoon is greatest at higher latitudes. From the repetitive nature of the pattern as observed the heating rate is consistently large in that local time sector. The morning sector has high speed plasma flow also but generally not as large as the afternoon sector. Thus, the large increases in heating rate observed previously directly over Chatanika are due in large part to simple expansions and contractions of the auroral oval. Further, since Chatanika is typically in the lower part of the oval the heating rates should be much greater in the poleward part of the oval. The cross comparisons of Millstone Hill and Chatanika radar data is still on progress. On average the electric fields observed from Millstone Hill are somewhat smaller than those observed at the same magnetic latitudes from Chatanika. A suggestion from model studies is that the offset of the geomagnetic pole from the geographic pole and a further offset of the center of the oval to be several degrees antisunward of the geomagnetic pole introduces a strong longitudinal variation in the magnetic latitude of the oval. So, some longitude sectors, such as Chatanika, penetrate more deeply into the oval than other locations with the same magnetic latitude.

Final Report

on

AFOSR Contract 77-3435

Energy Input to the Auroral Ionosphere

Submitted by

J. R. Doupnik
Center for Atmospheric and Space Sciences
Utah State University
Logan, Utah 84322

29 February 1980

1. Scientific Objectives

The proposal was to aid studies of the high latitude ionosphere particularly with regard to Joule heating processes. Joule heating is the product of the height integrated Pedersen conductivity of the plasma, which is proportional to the plasma density, and the square of the electric field present, which is measured by observing the plasma drift velocity transverse to the geomagnetic field. The Chatanika radar has been used to measure these quantities.

At the time of the proposal we were evolving the experimental method, using the Chatanika radar, from measuring the local (overhead) plasma parameters to measuring similar parameters over a wide range of magnetic latitudes. The reason for the change of method was to help answer the question of how much of the large variations of electric fields, currents, and Joule heating seen with the local experiments were due to just temporal developments and how much was due to a simple geographical expansion/contraction of the auroral oval. If the large variations were simply confined to small spatial regions or short time periods then the overall energy deposition in the ionosphere would be much less than the larger peaks observed locally. The experiments probing over a wide range of latitudes tend to smooth over small scale features and hence provide a more representative measure of the overall plasma parameters.

For energy input to the atmosphere by Joule heating the dominant physical factor has been found to be the strength of the electric field (i.e., the motions of the ionospheric plasma through the nearly stationary neutral gas). Both the conductivity and electric field change by large factors but the dependence of the Joule heating rate on the square of the electric field strength makes the electric field the most critical factor.

In the design of the experiments with the steerable dish antenna the conductivities are obtained from electron densities in the E region of the ionosphere while the electric fields are obtained from the F region. To cover a wide range of latitudes with acceptable time resolution the E region measurements were curtailed.

Two series of experiments were conducted with the Chatanika radar in Alaska; one in January 1978 and the second in June 1978. An objective of the June series was to further study the global pattern versus temporal fluctuation problems by simultaneously operating the Millstone Hill radar located in Massachusetts. Both radars would probe the same range of magnetic latitudes. An exploratory trip to Millstone Hill was made in May 1978 to learn how that system functioned. We then designed experiments which were executed successfully by Dr. Wand of Millstone Hill.

The raw radar data were recorded on magnetic tape and processed on the CASS Computer Facility computer to give geophysical parameters of plasma densities and drift velocities. Examples of the velocity data (i.e., electric fields) are shown in Figures 1-4; the first two are detailed velocity flow data and the second two are averages over the available data.

A finding from these and subsequent similar experiments is that the electric field pattern (strength and direction) is surprisingly smooth over large ranges of latitudes and over long periods of local time. The local afternoon sector (22 hours UT is local noon at Chatanika) is characterized by very strong electric fields which increase rapidly with latitude. Small changes in the diameter of the auroral oval due to substorms or fluctuations in the solar wind produce large variations of the field strength over Chatanika without necessarily altering the overall

electric field pattern. This means the Joule heating during the afternnon is greatest at higher latitudes. From the repetitive nature of the pattern as seen over the several days of observations during each series of experiments we can say that the heating rate is consistently large in that local time sector. The morning sector has high speed plasma flow also but generally not as large as the afternoon sector.

Thus, the large increases in heating rate observed previously directly over Chatanika are due in large part to simple expansions and contractions of the auroral oval. Further, since Chatanika is typically in the lower part of the oval the heating rates should be much greater in the poleward part of the oval.

The cross comparisons of Millstone Hill and Chatanika radar data is still in progress. On average the electric fields observed from Millstone Hill are somewhat smaller than those observed at the same magnetic latitudes from Chatanika. An example of this effect is shown in Figures 3 and 4. Below each panel of experimental data are patterns predicted by a model (Sojka, Foster, Raitt, Schunk, Doupnik. 1979). A suggestion from the model studies is that the offset of the geomagnetic pole from the geographic pole and a further offset of the center of the oval to be several degrees antisunward of the geomagnetic pole introduces a strong longitudinal variation in the magnetic latitude of the oval. So, some longitude sectors, such as Chatanika, penetrate more deeply into the oval than other locations with the same magnetic latitude.

Figure captions

Figure 1. Detailed plasma flow vectors as observed on two consecutive days in June 1978 at Chatanika Alaska (65° Λ). A dot marks the base of each vector. Magnetic coordinates are used where north is up and east is to the right on these plots. For conversion to electric fields, a flow speed of 1 km/sec is equivalent to an electric field strength of 50 mV/m. Local noon is at 22 hours UT.

Figure 2. Detailed plasma flow vectors observed on two consecutive days in December 1978 at Chatanika, Alaska. The format is the same as for Figure 1.

Figure 3. A composite average of several days of plasma flow data taken in June 1978. These data are plotted in geographic coordinates with North up on the figure. The lower panel represents model calculations of plasma flow by Sojka et al., 1979.

Figure 4. Similar to Figure 3 except using Millstone Hill data and the appropriate location for this radar in the model calculations. Local noon is 17 hours UT. Note the strong differences of flow strength between Figures 3 and 4 due to the longitude separation of the stations.

2. Travel

1 man trip to Millstone Hill Radar (near Boston) to develop joint experiments.

1 man trip to Chatanika Radar (Fairbanks) to conduct experiments.

3. Persons supported

J. R. Doupnik
J. C. Foster
G. S. Stiles

4. Technical presentations resulting form work performed on this grant.

"A Review of Incoherent Scatter Radar Measurements of Magnetospheric Electric Fields", Chapman Conference on Magnetospheric Substorms, Los Alamos, 1978.

"Large Scale Convection of the High Latitude Ionosphere", (with J. C. Foster and G. S. Stiles), Fall AGU meeting, San Francisco, 1978.

"Incoherent Scatter Radar Studies of the Dayside High Latitude Ionosphere", (with J. C. Foster and G. S. Stiles), Fall AGU meeting, San Francisco, 1978.

"Detailed Comparison of Ionospheric Convection and Density", (with J. C. Foster and G. S. Stiles), Fall AGU meeting, San Francisco, 1979.

"Chatanika Radar Electric Field Observations: Measurements in Important Boundary Regions", (with J. C. Foster and G. S. Stiles), Fall AGU meeting, 1979.

"A Review of Magnetospheric Electric Fields", IUGG meeting, Canberra Australia, 1979.

"Prolonged Radar Observations of an Auroral Arc", G. S. Stiles, J. C. Foster, J. R. Doupnik, in press, J. Geophys. Res.

"High Latitude Convection: Comparison of a Simple Model with Incoherent Scatter Observations", J. J. Sojka, J. C. Foster, W. J. Raitt, R. W. Schunk, J. R. Doupnik, in press J. Geophys. Res.; also presented at Fall AGU meeting, San Francisco, 1979.

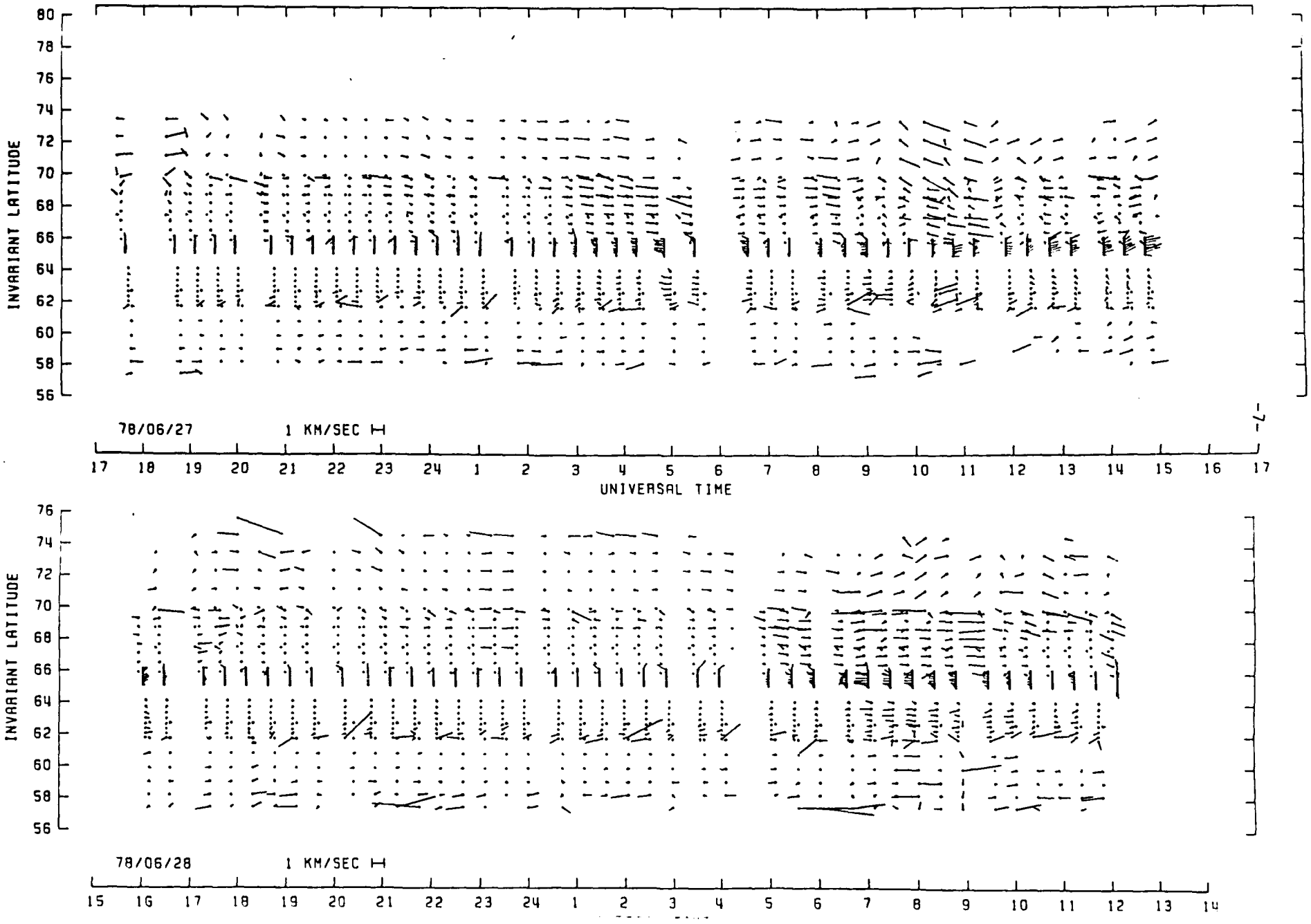
INVARIANT LATITUDE
80
78
76
74
72
70
68
66
64
62
60
58
56
78/06/27
1 KM/SEC H
17 18 19 20 21 22 23 24 1 2 3 4 5 6 7 8 9 10 11 12 13 14 15 16 17
UNIVERSAL TIME
INVARIANT LATITUDE
76
74
72
70
68
66
64
62
60
58
56
78/06/28
1 KM/SEC H
15 16 17 18 19 20 21 22 23 24 1 2 3 4 5 6 7 8 9 10 11 12 13 14

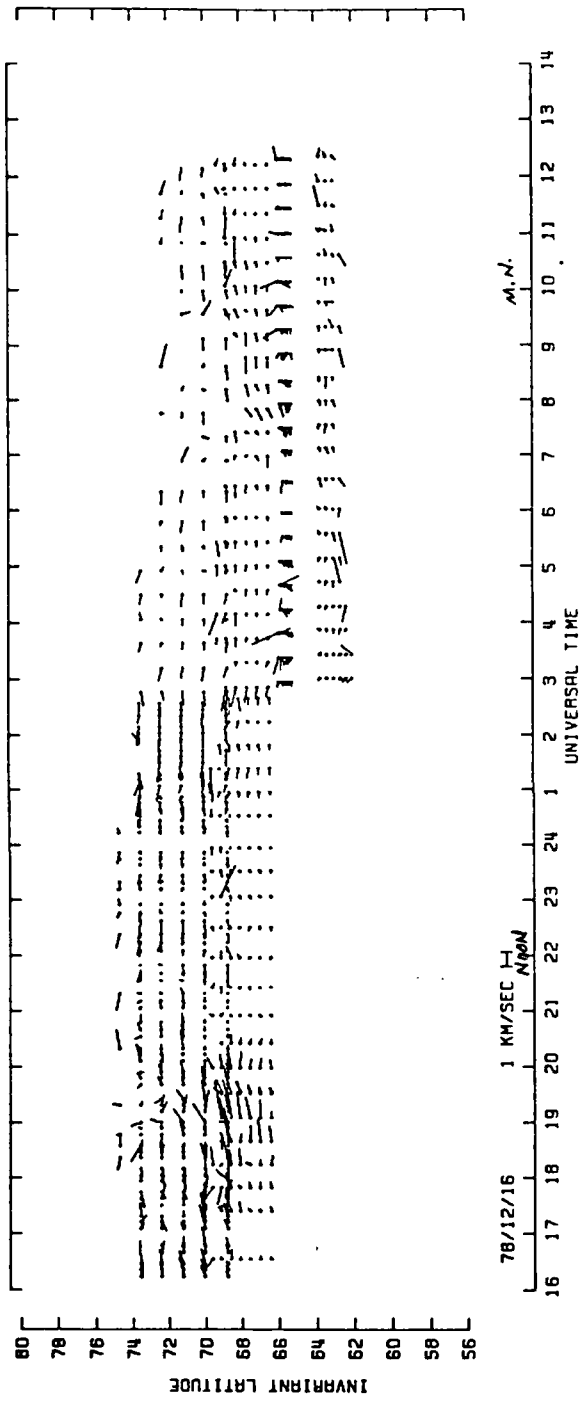
INVARIANT LATITUDE
80 78 76 74 72 70 68 66 64 62 60 58 56
78/12/16
1 KM/SEC H
NOON
16 17 18 19 20 21 22 23 24 1 2 3 4 5 6 7 8 9 10 11 12 13 14
M.N.
UNIVERSAL TIME

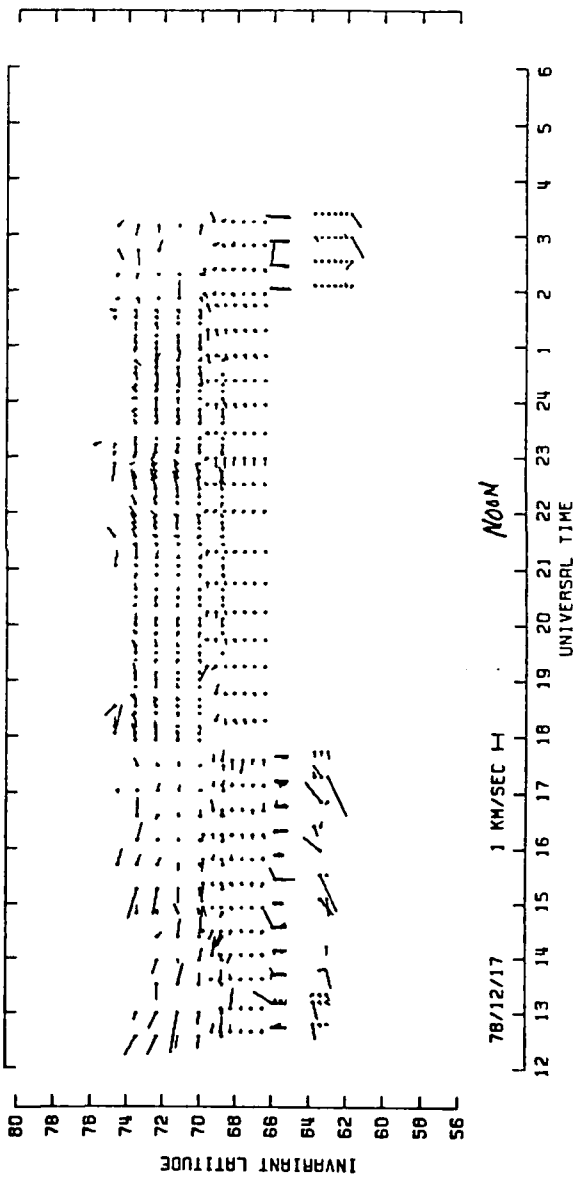
INVARIANT LATITUDE
80 78 76 74 72 70 68 66 64 62 60 58 56
78/12/17
1 KM/SEC H
NOON
12 13 14 15 16 17 18 19 20 21 22 23 24 1 2 3 4 5 6
UNIVERSAL TIME

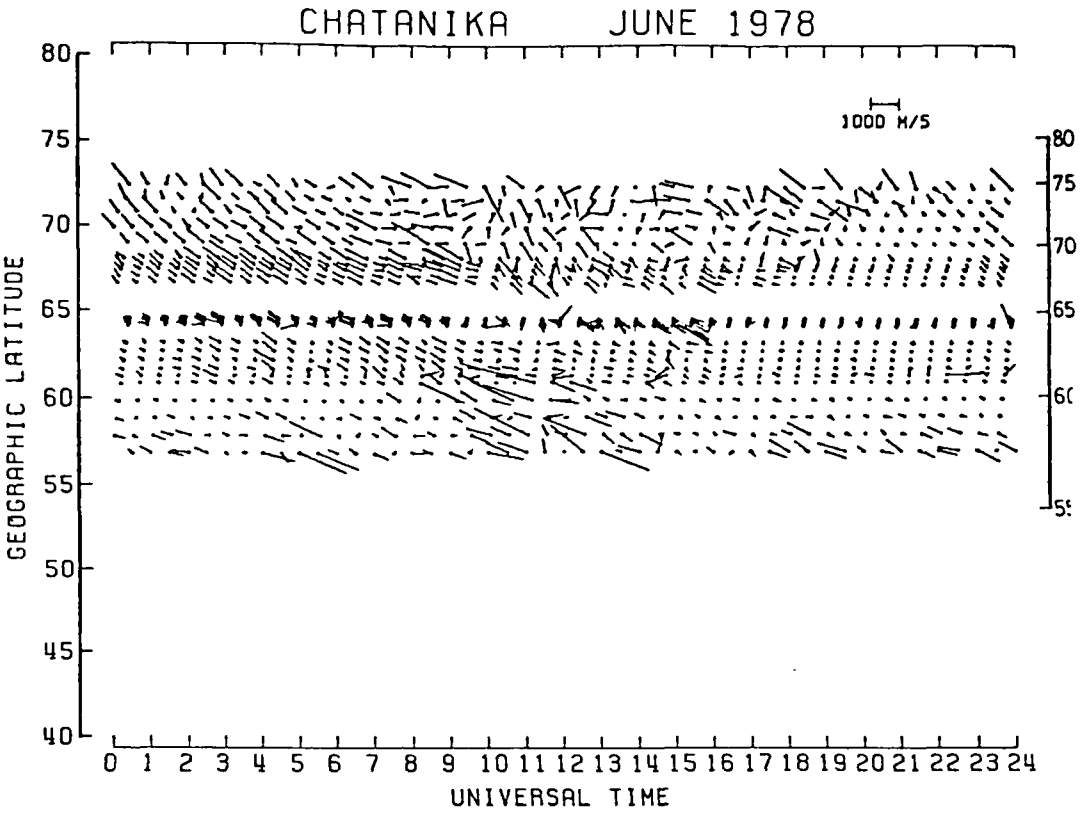
CHATANIKA JUNE 1978
1000 M/S
GEOGRAPHIC LATITUDE
80
75
70
65
60
55
50
45
40
0 1 2 3 4 5 6 7 8 9 10 11 12 13 14 15 16 17 18 19 20 21 22 23 24
UNIVERSAL TIME

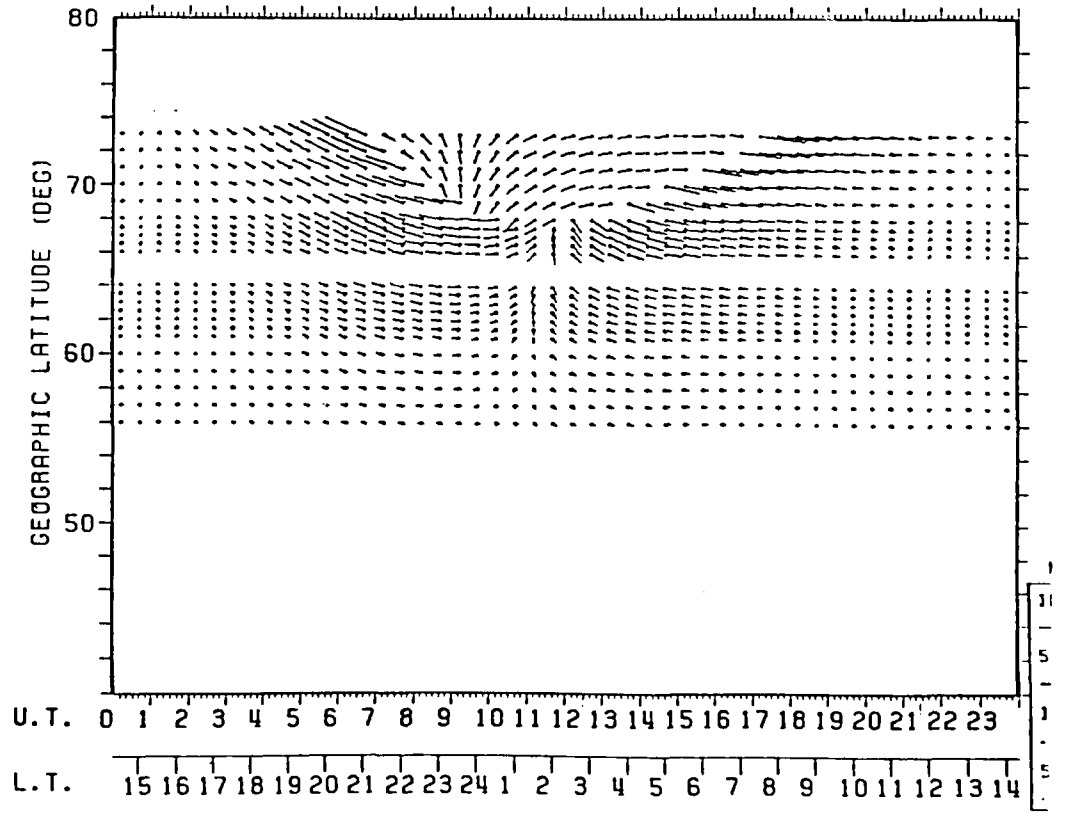
GEOGRAPHIC LATITUDE (DEG)
80
70
60
50
U.T. 0 1 2 3 4 5 6 7 8 9 10 11 12 13 14 15 16 17 18 19 20 21 22 23
L.T. 15 16 17 18 19 20 21 22 23 24 1 2 3 4 5 6 7 8 9 10 11 12 13 14

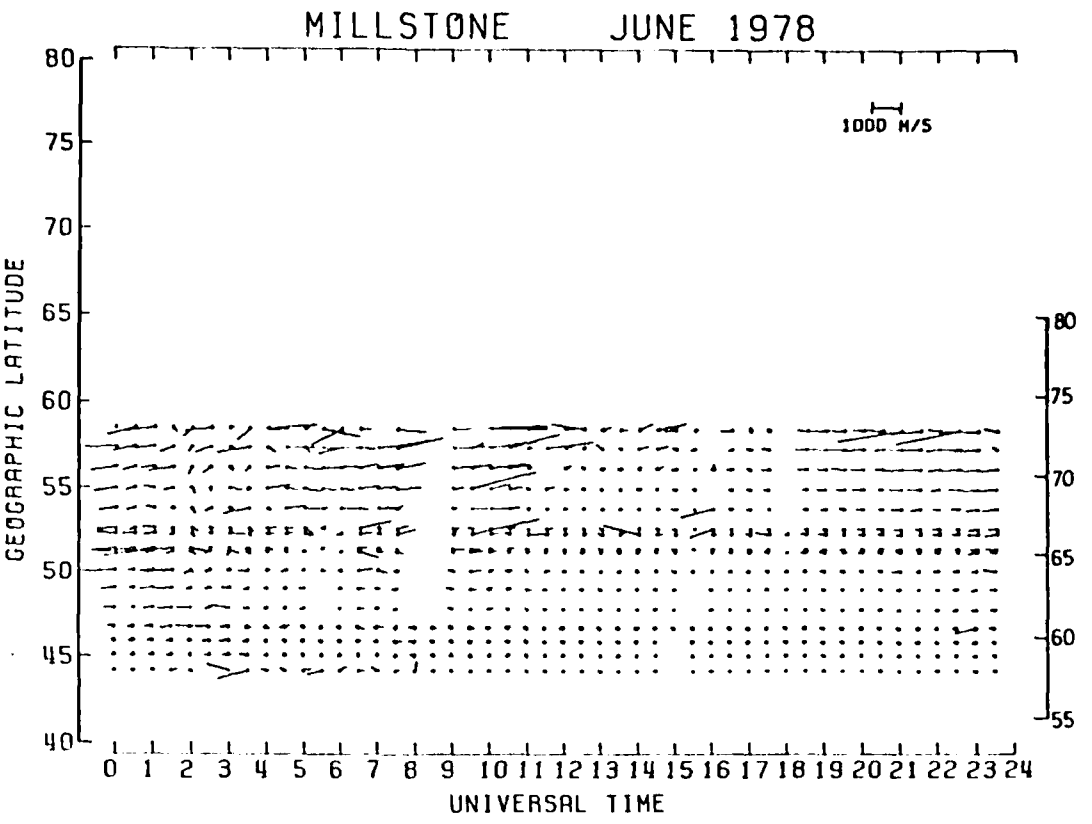
MILLSTONE JUNE 1978
1000 M/S
GEOGRAPHIC LATITUDE
80
75
70
65
60
55
50
45
40
0 1 2 3 4 5 6 7 8 9 10 11 12 13 14 15 16 17 18 19 20 21 22 23 24
UNIVERSAL TIME

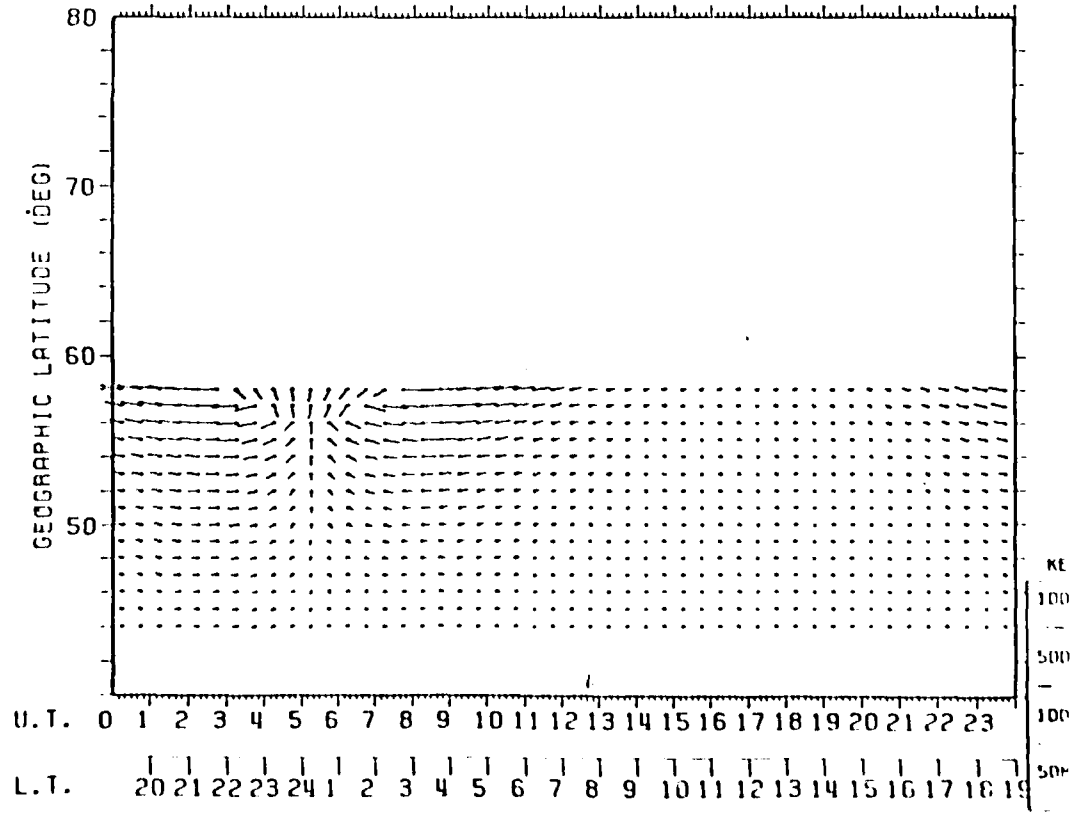
GEOGRAPHIC LATITUDE (DEG)
80
70
60
50
U.T. 0 1 2 3 4 5 6 7 8 9 10 11 12 13 14 15 16 17 18 19 20 21 22 23
L.T. 20 21 22 23 24 1 2 3 4 5 6 7 8 9 10 11 12 13 14 15 16 17 18 19
KE
100
500
100
50

5. Papers currently in press in J. Geophys. Res.

PROLONGED RADAR OBSERVATIONS OF AN AURORAL ARC

G. S. Stiles, J. C. Foster, and J. R. Doupnik

Center for Atmospheric and Space Sciences, Utah State University, Logan, Utah 84322

Abstract. On January 29, 1977, an auroral arc remained in the field of view of the Chatanika incoherent scatter radar for about 1 hour. Prolonged measurements were made of the line-of-sight velocities and densities from roughly 80- to 250-km altitude within and on both sides of the arc. From these basic measurements electric fields, conductivities, currents, and heating rates were calculated. In spite of the fact that the arc changed its appearance considerably over the hour, the measured and calculated parameters remained qualitatively very much the same. The northward electric field was very strong and showed a latitudinal profile similar to that frequently observed on satellites. One hundred (100) km equatorward of the arc the field was ~30 mV/m; from that point it increased to over 100 mV/m at the equatorward edge of the arc. The field then dropped sharply to ~30 mV/m within the arc. The northward field did not change across the poleward edge of the arc, indicating that there was no polarization effect. The latitudinal profile of the calculated horizontal currents suggests that the major downward field aligned currents are located in the region equatorward of the arc and the upward currents at the equatorward edge of the arc. The integrated joule heating rate peaked just equatorward of the arc, reaching a value of over 150 ergs cm^{-2} s^{-1}; inside the arc it dropped to 20-40 ergs cm^{-2} s^{-1}. The particle heating rate was negligible outside and was 10-30 ergs cm^{-2} s^{-1} inside the arc. The joule heating always exceeded the particle heating.

1. Introduction

During the past decade there has been considerable theoretical work done on the sources and structure of auroral arcs [see Akasofu, 1977, and references therein]. This work was based primarily upon previous visual and satellite

observations. Recently ground-based methods of investigating the auroral ionosphere have become increasingly sophisticated and have yielded important information on the features or arcs. Anderson and Vondrak [1975] have reviewed early work on field-aligned currents. Rocket measurements have been made by Carlson and Kelley [1977], Kelley and Carlson [1977], Evans et al. [1977], Maynard et al. [1977], and Arnoldy [1977]. Incoherent scatter radar measurements of several arcs at Chatanika, Alaska, have been reported by de la Beaujardiere et al. [1977]. In this paper we report new and unique observations of an auroral arc made also with the Chatanika facility.

In our January 1977 expedition to Chatanika we had the opportunity to observe a fairly well defined premidnight auroral arc for a period of about 1 hour. We succeeded in obtaining measurements of the electron density and line-of-sight velocities in a region extending roughly 100 km equatorward to 20 km poleward of the arc. From these measurements we can estimate the electric fields, conductivities, currents, and heating rates.

Our results reveal some of the strongest electric fields adjacent to (>100 mV/m) and within (~30 mV/m) an arc that have been observed with the radar and provide the first clear ground-based example of the latitudinal electric field profile commonly seen by satellites in the evening sector auroral zone. The northward field rose from a value typical of the evening convection field (~30 mV/m) 100 km equatorward of the arc to over 100 mV/m immediately equatorward of the arc. The fields equatorward of the arc were most intense near the arc and decreased with increasing distance from the arc. At the equatorward edge of the arc the field dropped sharply to ~30 mV/m. The field maintained this value throughout the arc and across its poleward edge, indicating that the decrease of the field was not due to the accumulation of polarization charges at the edges of the arc. The gradual rise and sharper drop of the electric field have frequently been seen on satellites adjacent to auroral particle fluxes [Burch et al., 1976a]. Similar, but less well defined, electric field profiles have been seen in earlier unpublished Chatanika data.

Strong height-integrated currents (>1 A/m) were associated with these fields. The gradients in the horizontal currents were most pronounced outside of the arc and suggest that the upward current is located primarily at the equatorward

edge of the arc and the downward current equatorward of the upward current.

These results will be described in detail in the following sections. Note especially that the essential features of the arc remain qualitatively the same throughout the nearly 60 minutes of observations, in spite of the fact that the arc undergoes considerable changes in position and appearance.

2. Experimental Procedure

The Chatanika incoherent scatter radar facility, run by SRI International, is located 44 km northeast of Fairbanks, Alaska. The geomagnetic latitude of the station at ground level is 64.85°. The transmitter produces approximately 3 MW at 1290 MHz and operates into a 27-m fully steerable dish. (The system is described by Leadabrand et al. [1972] and Baron [1977]. The latter reference pays particular attention to the newer signal processing techniques that are available.) The width of the antenna beam is about 1 km at 100-km altitude and about 2 km at 200-km altitude. The received signal was integrated for 15 seconds for each set of measurements.

At the time the arc appeared we were conducting an experiment designed to study the altitude dependence of ion velocities. The antenna was pointed magnetically east and was moved between several fixed positions at elevations ranging from 37° to 64°. One position pointing up the field line (used to measure field-aligned velocities) was also included. With the eastward orientation of the antenna we were in an ideal position to measure the east-west ion velocities and thus the northward component of the electric field.

The arc drifted into the radar beam at approximately 0942 UT (≈2215 MLT) on January 29, 1977. We maintained the operational mode described above for the next half hour as the arc continued to move in and out of the beam. The antenna was then put into a mode whereby it would scan in azimuth across the arc at an elevation of 60°. The scan ranged from roughly 15° north of magnetic east to 35° south. The antenna was left in this mode for the remaining half hour of operation.

The basic plasma parameters yielded by the radar system are the electron density, deduced from the strength of the returned signal, and the ion velocity, deduced from the Doppler shift of the signal. From the density as a function of

altitude the height-integrated conductivities can be derived with the aid of suitable neutral atmosphere models and estimates of collision rates. We used the same model and rates as used by Brekke et al. [1974b].

Throughout the experiment, densities at the altitudes of interest remained good, and the signal-to-noise ratios were usually well above 20% both inside and outside the arc. Recent Monte Carlo calculations [J. R. Doupnik, unpublished manuscript, 1979] indicate that the uncertainties in the measured line-of-sight velocities should be less than 25 m/s under these conditions; this uncertainty is at least an order of magnitude less than the velocities discussed below.

Rigorous calculation of the vector electric field requires that all three components of the ion velocity be measured. In our experiment we essentially measure only the eastward and field-aligned velocity components, and a method developed by Doupnik et al. [1977] is used to estimate the total field. This method, which has also been used by de la Beaujardiere et al. [1977], calculates components of $\vec{E}$ perpendicular to $\vec{B}$ by using the change in the measured line-of-sight velocity between the F and the E regions.

In the F region, where ion-neutral collisions are negligible, the measured line-of-sight velocity is assumed to be due entirely to the component of $\vec{E}$ perpendicular to the line-of-sight. In the E region, where collisions are important, the measured velocity is also affected by the neutral wind $\vec{U}$, the component of $\vec{E}$ parallel to the line-of-sight, and the conductivity. Since the component of $\vec{E}$ perpendicular to the line-of-sight is known from the F region velocity measurements, we can calculate the parallel component if a value for $\vec{U}$ and a conductivity model are assumed. If we further assume that the component of $\vec{E}$ parallel to $\vec{B}$ is negligible, we can calculate the components of $\vec{E}$ perpendicular to $\vec{B}$. The effects of these assumptions are discussed by de la Beaujardiere et al. [1977] and Doupnik et al. [1977]. Our estimates of the uncertainties stated below are based upon the solutions of the equations given in those papers using various values for the quantities which must be assumed (e.g., neutral wind velocities and collision rates).

In the results that follow, the component of the field least subject to error is the northward component E_n, which is calculated primarily from the F region velocity measurements. The eastward component E_e depends significantly upon the E

region neutral winds and collision rates and may be subject to considerable error.

In the region equatorward of the arc the measured velocities (≥1500 m/s) and the calculated fields (≥100 mV/m) are large. Consequently, typical values of neutral winds, which are ≤1000 m/s even in disturbed times [Brekke et al., 1973, 1974a; Rino et al., 1977], would not have a major qualitative effect on our results. The neutral wind $\vec{U}$ would have to be in excess of several kilometers per second to completely account for our calculated eastward electric field E_e.

Within the arc, however, where the fields are much smaller (≈30 mV/m), the effect of the neutral wind on the calculated value of E_e can be very large. If we assume that $\vec{U}$ may reach several hundred meters per second (rare, but not unknown [Brekke et al., 1974a] the uncertainty of E_e within the arc is of the order of E_e itself. The uncertainty in E_n within the arc is still small, since E_n is derived from observations in the collision-free F region. For the results presented below we have assumed $\vec{U} = 0$.

The collision rate, like the neutral wind, has little effect upon E_n but can change E_e drastically, even in the region of large fields outside of the arc. An uncertainty in the collision rate by a factor of 2 yields, again, an uncertainty in E_e roughly equal to E_e itself. In the results below we follow Brekke et al. [1973] and use a collision rate of $7.5 \times 10^{-10} N_n$ cm^{-3} s^{-1}, where N_n is the neutral density.

The electric field, once calculated, is combined with the height-integrated conductivities to yield the height-integrated currents and the joule heating rates. (The methods are outlined by Brekke et al. [1974b] and Banks [1977].) The currents and Joule heating are uncertain by roughly a factor of 2 owing to the uncertainty in E_e and the conductivities. The heating due to the influx of particles is calculated from the measured density and an assumed energy input of 28.8×10^{-12} ergs per electron-ion pair produced [Banks, 1977].

3. Gross Results

The auroral arc to be discussed below was observed between 0930 annd 1040 UT on January 29, 1977. Geomagnetic activity had been very low until late on the 28th but then picked up substantially. Kp for the 3-hour periods preceding our observations was 5+, 5-, 3+, 3+, and 3-. The College magnetometer showed positive and

negative bays of several hundred gamma from ~0700 to 1200 UT. The Chatanika riometer also showed significant activity.

The Chatanika all-sky camera recorded active aurora overhead for several minutes prior to 0915 UT. At this time the arcs broke up and then gradually faded from view over the next 10 minutes. By 0930 another bright arc had formed to the north of Chatanika. This arc drifted equatorward slowly and somewhat erratically. The arc first came within the radar beam at ~0942:30 UT (see Figures 1 and 2). The arc was in and out of the beam for the next hour. Except for the period ~1004-1010, when it split into two main parts, the arc was fairly well defined and did not form any spirals. Bulges occasionally passed overhead and several smaller features split off the main arc. From all-sky camera photos we estimate that the arc ranged in width from ~10 km when it was quiet to over 20 km as it became more active.

The basic measurements are shown in Figure 3, which presents the density integrated from 80- to 170-km altitude and the line-of-sight velocities measured in the E and F regions. As the arc approaches (~0920-0942) there is a gradual decrease in the integrated density and a marked increase in the velocities. (Since this decrease is not mirrored when the arc finally recedes poleward after 1030 UT, we feel that it may only be the decay of the particles remaining from the previous auroral activity.) Just equatorward of the arc, at 0942, the integrated density is ~0.7 x 10^{12} cm^{-2}. The small increases in the integrated density just prior to this time may be due to the passage through the beam of small, faint arcs that are just visible on the all-sky camera pictures.

The line-of-sight velocities equatorward of the arc reach ~1500 m/s in the F region and ~800 m/s in the E region. The E region velocity differs from that in the F region due to the higher collision rate in the E region and also possibly to the presence of an eastward electric field and a nonzero neutral wind. This difference, as described above, is the basis for estimating the components of $\vec{E}$ perpendicular to $\vec{B}$.

The entry of the arc into the radar beam at 0942:30 is clearly marked by the simultaneous jump of the integrated density to ~6 x 10^{12} cm^{-2} and the drop of the velocities to under 500 m/s. (Small filamentary arcs may have passed through the beam at ~0936 and ~0940 UT.) For the remaining hour, as the plot shows, the arc continued to drift in and out of the radar beam.

The exits and entries, as determined from the density measurements, agree well with the position of the radar beam as plotted on the all-sky camera pictures. The horizontal bars on Figure 3 are used to denote when the radar was looking at the arc; these bars have been lined up with the times when the integrated density crosses 1.6×10^{12} cm^{-2}. The letters E and P refer to times when the radar was looking equatorward or poleward of the arc, respectively (this determination becomes difficult when the arc fades and reforms elsewhere, as near 1005 UT).

Figure 3 shows particularly well that over the hour the basic features of the arc remained qualitatively very much the same. Each passage of the equatorward edge of the arc through the radar beam was accompanied by density and velocity changes of comparable size. Note particularly the increase of the velocities during the initial approach and entry prior to ~0942 and the decrease following the final exit and recession at ~1030. (We do not have sufficient information to determine whether the increase in velocity as the arc approaches and the decrease as it recedes are spatial or temporal effects. Since the arc retains much the same appearance as it initially approaches, however, it may be more likely that it is a spatial effect.) The strong anticorrelation between the velocities and densities is presumably due to the behavior of the electric field within and outside the arc and is discussed in detail below.

Figure 4 shows electron density profiles derived from the line-of-sight measurements. Profile (a) was taken approximately 100 km equatorward of the arc; the peak of the density is ~120 km. By profile (b), which was taken during the last 3-minute period prior to the entry of the arc into the radar beam, the density peak had risen to ~125 km. Furthermore, although the peak density remained roughly the same, the densities both below and above the peak were depleted (see the superimposed profiles in (d)). We are unable to say at this time whether the depletion is due to the presence of the large electric fields or is simply a decay of the particles remaining from the previous activity. Within the arc (profile (c)) the peak density has increased to over 10^6 cm^{-3}. The altitude of the peak has dropped to ~102 km, suggesting that the incident particles peak at energies of ~10 keV. The densities show increases from ~90 to over 200 km, indicating further that significant fluxes from ~1 to over 10 keV are present.

In Figure 5 we present the components of $\vec{E}$ perpendicular to $\vec{B}$, E_n, and E_e, calculated as described in the last section. Recall that E_e is subject to an uncertainty of the order of E_e itself, but that E_n should be accurate to, in the worst case, $\sim\pm15\%$. The fields, as expected, follow the velocities and increase in magnitude as one approaches the arc from the equatorward side; note that E_e is <0 and thus westward. Immediately equatorward of the arc the magnitudes of E_n and E_e are $\geq$120 mV/m; these are some of the largest fields that we have observed with the radar. The direction of the field in this region is to the northwest. E_n, the component which is less erratic and most certain, is poleward throughout the period of observation.

The decrease in the magnitude of the field occurs just at the edge of the arc. The northward component drops to $\sim$+30 to +40 mV/m within the arc; the eastward component fluctuates between $\sim\pm30$ mV/m. The northward component, which is fairly steady, is considerably larger than the fields previously reported within the arcs.

Between $\sim$0946 and 0949 the poleward edge of the arc passed clearly out of and back into the radar beam. Our measurements show that E_n does not change across this boundary; this result, as we shall see below, argues strongly against the presence of any polarization field within the arc.

Figure 6 shows the height-integrated conductivities and currents. Of particular interest is the fact that there is no obvious enhancement of the conductivities equatorward of the arc. The ratio of Σ_H to Σ_p is $\sim$1 immediately outside the arc. Within the arc Σ_H/Σ_p ranges from $\sim$1 to $\sim$3, the upper limit being obtained when the densities were particularly high ($\sim$0942-0950).

The height-integrated currents, calculated from E_n, E_e, Σ_H, and Σ_p, are given in Figure 6b. Equatorward of the arc the northward component is directed toward the arc and increases as the arc is approached. J_e is predominantly eastward throughout the observation, indicating that the arc is embedded in the region of the eastward electrojet.

On the initial passage into the arc $\sim$0942-0946 UT, J_n drops sharply and becomes strongly southward. This is apparently the result of the initially high Hall conductivity and the relatively strong eastward field (recall, however, that the uncertainty in J_n is of the order of $\sim$1 A/m at this time). During this same period, J_e becomes strongly positive ($\geq$3 A/m); this measurement agrees well with the simultaneous

strong positive deflection in the H component of the local magnetometer.

After the decay of the initially high density and Hall conductivity (~1002 UT), J_n becomes northward again and remains so for most of the remainder of the observations. Within the arc, J_n is ~0.5-1.0 A/m, and equatorward of the arc, J_n is ~0.5-2.0 A/m. Note that the largest values of J_n always appear at the equatorward edge of the arc. Far equatorward of the arc, J_n is ~0.3-0.5 A/m.

The eastward component of the current within the arc ranges from ≥3 A/m during particularly high densities, as noted above, to ~0.3 A/m. In contrast to J_n, J_e tends to show an initial decrease upon an equatorward exit from the arc (~1017, ~1029). As the arc finally recedes poleward near 1040 UT, J_e drops to ~0.

The horizontal (H) and vertical (Z) components measured by the Poker Flat magnetometer (located ~1 km from the radar) are shown in Figure 7. The H displacement is predominantly positive prior to ~1100 UT, indicating that Chatanika was in the premidnight sector until this time. The H component is strongly positive from ~0935 to 1030 UT, roughly the time during which the arc was overhead and we measured an eastward current.

Height-integrated joule (Q_J) and particle (Q_p) heating rates are shown in Figure 8. The value for joule heating is uncertain by a factor of ~4, as mentioned earlier. The largest value of joule heating, ~160 ergs cm^{-2} s^{-1}, occurs just equatorward of the arc, where the electric fields are largest. Q_J drops sharply inside the arc but is still significant at ~20-40 ergs cm^{-2} s^{-1}. The heating due to the influx of particles is insignificant outside (<1 erg cm^{-2} s^{-1}) but becomes appreciable (~10-40 ergs cm^{-2} s^{-1}) within the arc when the densities are high. When the densities decrease, due presumably to a falloff of the incident flux, Q_p drops to ≤ 10 erg cm^{-2} s^{-1}.

4. Detailed Results

In this section we shall take a closer look at the distribution of the fields and currents near the boundaries of the arc. Knowledge of these features is essential for understanding both the mechanism which produces the arc and the interaction of the precipitating particles with the ionosphere.

Figure 9 shows superimposed plots of the integrated density and the northward component of the field for each clear passage of the equatorward edge of the radar beam. Figure 10

shows the same quantities for two of the poleward passages. The plots have been aligned using the times where the integrated density crosses 1.6×10^{12} cm^{-2} (these times are shown in Figure 3). Where necessary the curves have been plotted with time increasing to the left so that all crossings will have the same orientation.

Two of the equatorward passes shown in Figure 9 either began or ended a considerable distance from the arc ($\sim$100 km, from all-sky pictures). In both passages the northward field increases from $\sim$40 mV/m to 120 mV/m as one approaches the arc. (As is noted above, this change appears to be spatial, although we cannot definitely rule out a temporal change.) These results indicate that there is a field equatorward of the arc (but still associated with it) that is considerably greater than the background field of $\lesssim$ 40 mV/m.

The electric field reaches its peak just at the equatorward edge of the arc. Upon entry the field drops at the same time that the density rises. After the entry into the arc has been completed (determined by the levelling off of the density) the northward field ceases to decline and remains relatively constant inside the arc.

The crossing of the poleward boundary of the arc is particularly interesting. Unfortunately, we have only two good examples of such a crossing (the other two apparent crossings near 1005 and 1025 took place while the arc was fading and reforming), but both show (Figure 10) that there is virtually no change in the northward component of the field across the poleward edge: the fields outside and inside the arc are nearly identical. The importance of this observation, which implies that there is no polarization field established within the arc at these times, will be discussed below.

The northward current, which is also shown in Figures 9 and 10, is of interest because its profile can provide information on the distribution of field-aligned currents through the relation $J_{\parallel} = (dJ_n/dn)$. On the equatorward side, as the arc approaches, J_n shows a slow increase matching the increase in $\vec{E}$. If we assume that this increase takes place over a distance of roughly 100 km (a reasonable estimate, based on all-sky photos), then we have a downward field-aligned current of $\sim(1 \text{ A/m})/(10^5 \text{ m}) = 10^{-5}$ A/m^2 in the region equatorward of the arc. As we shall see in the next section, this is in keeping with other estimates of such currents.

The decrease in J_n, like that of the field, occurs right at the edge of the arc: the density

and current gradients overlap. Within the arc the current is relatively constant. This result implies that the major upward current is located at the equatorward edge of the arc. To estimate the magnitude of the upward current, we need to know the width of the region over which the decrease in the horizontal current takes place. We unfortunately do not have sufficient temporal resolution in the all-sky pictures to measure this distance. We would expect this region to be much less than 100 km, however, and would thus expect the upward current to be stronger than the downward current calculated above.

The changes in the current on the passages of the poleward edge of the arc through the radar beam are difficult to decipher because of the relatively rapid temporal changes in the density (and thus conductivities) that are occurring at that time. These changes in turn cause large-temporal variations in J_n that mask any spatial variations.

5. Comparison With Earlier Results

In this section we shall briefly summarize the results of our observations and then compare them with some of the more recent experimental work.

a. Our Results

Electric fields. As the arc is approached from an equatorward distance of $\geq$100 km the northward field increases from $\leq$40 mV/m to $\geq$100 mV/m; the eastward component of the field decreases from $\geq$-10 mV/m to $\sim$-100 mV/m. Within the arc, E_n is $\sim$30 mV/m and fairly steady; E_e fluctuates between $\sim\pm$30 mV/m. The northward component shows little change during two clear crossings of the poleward edge of the arc. The major gradients in the field occur equatorward of or at the equatorward edge of the arc.

Currents. The height-integrated northward current far equatorward of the arc is $\sim$0.2-0.5 A/m; J_e far equatorward is about zero. As the arc is approached, J_n increases to 1.4-1.8 A/m and J_e to 0.5-1.0 A/m. These increases are due to an increase in the electric field alone, since the conductivity equatorward shows no enhancement. Within the arc, J_n drops to $\sim$0.6-1.0 A/m, and J_e increases to 1-2 A/m (there is a period of higher conductivities inside the arc when $J_n \leq$ -2 A/m and $J_e \sim$ 4 A/m). The major spatial gradients of the currents are again equatorward of or at the equatorward edge of the arc.

Heating. The height-integrated joule heating far from the arc is $\lesssim$20 ergs cm^{-2} s^{-1}; the particle heating outside of the arc is $\lesssim$1 erg cm^{-2} s^{-1}. Just equatorward of the arc, where the fields are largest, the joule heating is also largest and is $\gtrsim$150 ergs cm^{-2} s^{-1}. Within the arc the joule heating is typically $\sim$20-40 ergs cm^{-2} s^{-1} but rises to $\sim$60 ergs cm^{-2} s^{-1} during the period of high density. In the same period the particle heating rate is $\sim$40 ergs cm^{-2} s^{-1}. In the remainder of the observations within the arc the particle heating rate is $\lesssim$10 ergs cm^{-2} s^{-1}. The particle heating rate is always less than the joule heating rate.

b. Earlier Work

There have been several recent experimental studies of the fields, particles, and/or currents associated with auroral arcs. Carlson and Kelley [1977] examined the particle fluxes, fields, and currents with instruments carried on board a rocket; Evans et al. [1977], also using a rocket, studied fields, fluxes, conductivities, currents, and heating rates; de la Beaujardiere et al. [1977] looked at particles, fields, and currents with the Chatanika radar; Casserly and Cloutier [1975] and Arnoldy [1977], again with rocket-borne instrumentation, examined field-aligned currents in the vicinity of auroral arcs.

A comparison of our field measurements with those of the other investigators shows both similiarities and significant differences. Qualitatively, the northward component of the field showed similar variations across the equatorward edge of the arcs in all four experiments. In each case the field drops sharply at this boundary.

Quantitatively, however, there is considerable variation from case to case. The northward field just outside the arc ranges from $\sim$+20 mV/m [de la Beaujardiere et al., 1977] to $\gtrsim$100 mV/m (ours). Inside the arc the values range from $\sim$-80 mV/m [Carlson and Kelley, 1977] to $\sim$+30 to 40 mV/m (ours). These differences are not surprising in view of the wide range of intensities and forms that arcs may assume and the possible variations in the locations of the arcs relative to other features of the auroral oval.

The fact that Carlson and Kelley [1977] show a negative E_n within the arc may be due to local time effects. In the single instance of a southward field within an arc reported by de la Beaujardiere et al. [1977], the measurements were

made after local midnight. This suggests that Carlson and Kelley may have been looking at a postmidnight arc, while ours was a premidnight feature. If the arc were lying just along the Harang discontinuity, we might also expect to see the northward field change from positive to negative within the arc; this effect could occur prior to midnight in the poleward portion of the oval.

Our measurements do disagree qualitatively with the others at the poleward edge of the arc. Ours is the only case where E_n does not increase as the arc is exited across this boundary. The significance of this observation is discussed below.

Measurements of the eastward component of the electric field also varied widely (recall that the radar measurements of E_e are fairly uncertain). Equatorward of the arc the observed values ranged from roughly -100 mV/m (ours) to +20 mV/m [de la Beaujardiere et al., 1977]. Within the arc, E_e decreased in magnitude and for three of the observations was between $\sim$-10 and +10 mV/m; our measurements fluctuate from $\sim$-30 to +30 mV/m. Poleward of the arc, E_e was generally between $\sim$0 and -20 mV/m.

We doubt if the large value we obtain for the field equatorward of the arc is due to the presence of uncompensated neutral winds; such winds would need to have velocities of several kilometers per second to produce the measured field. It is possible that the collision rate we chose is too high; halving it would keep E_e in the range of $\sim\pm$ 40 mV/m.

Evans et al. [1977] and de la Beaujardiere et al. [1977], as well as ourselves, have calculated the horizontal components of the currents. All the calculations show an eastward current of $\lesssim$ 0.4 A/m equatorward of the arc. In the same region we see a poleward current of $\lesssim$1 A/m. De la Beaujardiere et al. [1977] find an equatorward current of $\sim$0.2 A/m, and Evans et al. see virtually no J_n.

Within the arc, Evans et al. [1977] also see little northward current. De la Beaujardiere et al. find that J_n increases to $\sim$0.4 A/m. In our calculations, J_n decreases to $\sim$0.8 A/m during most of the time and to $\sim$-2 A/m during the period of high density. We and Evans et al. [1977] both see a typically eastward component of $\sim$0.5 A/m inside the arc, which is about that observed outside (our J_e did approach 4 A/m during the period of high density). De la Beaujardiere et al. [1977], however, found that J_e decreased to $\lesssim$0.1 A/m

inside the arc. If we were forced to draw a consensus from these rather disparate results, we would say that the horizontal current outside of and within an evening arc is generally to the north and east.

Field-aligned currents are of particular interest, since they presumably link the arc to the region that accelerates the auroral particles. Radar experimenters must derive these currents by differentiating the horizontal currents, which themselves are subject to considerable error and often noisy. Rocket experimenters may do the same, may count the up- and down-going charged particles, or may use on-board magnetometers.

While we have not gone so far as to differentiate horizontal currents calculated from the arcs, the profiles of those currents, shown in Figure 9, indicate that there is a downward current located entirely equatorward of the arc with a magnitude of $\sim 10^{-5}$ A/m^2. (The presence of a downward current is suggested by the fact that the poleward current increases as the arc is approached; this increase is not accounted for by the variation in the eastward current.) A good estimate of the upward current at the equatorward edge is prevented by the fact that we do not know the width of the region over which the density rises and the current falls. If we choose to set an upper limit of 20 km on this width, then the upward current has a lower limit of $\sim$0.5 A/m/20 km $\sim 3 \times 10^{-5}$ A/m. Our results suggest that there is relatively little parallel current inside the arc. Due to rapid time variations we are unable to determine what happens at the poleward edge.

Casserly and Cloutier [1975], using a rocket-borne magnetometer, also found a downward current equatorward of an arc. In contrast to our results, however, they found the upward current to be distributed throughout the arc, rather than concentrated at one or both edges.

Evans et al. [1977] differentiate the horizontal currents to find $J_{\parallel}$. Although they get two different numerical results depending upon their assumptions, the two results are qualitatively similar. They find that the largest upward currents are located at the equatorward edge of the arc, as our results suggest. They also find evidence of a smaller upward current at the poleward edge. The presence of a downward current was not detectable in the somewhat noisy data.

Carlson and Kelley [1977] examined the upward and downward particle fluxes. They concluded that there was a downward current equatorward of the

arc and an upward current within and poleward of the arc.

Arnoldy [1977] calculated the parallel currents by looking at low energy electron fluxes. He found that the upward currents were concentrated at the two edges of the arcs with a smaller upward component in between.

Heating rates were only looked at by Evans et al. [1977]. Equatorward of the arc they observed joule heating rates of 10-15 ergs cm^{-2} s^{-1} and particle heating rates of ≤ 1 erg cm^{-2} s^{-1}. Within the arc they found these rates to be ~ 2 and ~ 30-35 ergs cm^{-2} s^{-1}, respectively.

These results are consistent with ours. Our joule heating rate outside the arc of ~ 180 ergs cm^{-2} s^{-1} is considerably larger than theirs owing to the fact that the electric fields we measured were 2 to 3 times larger. Our particle heating rates are comparable to theirs both inside and outside the arc.

In discussing the heating rates, Evans et al. [1977] note that the drop in their joule heating just matches the rise in the particle heating so that there is not an abrupt change in the total heating rate across the edge of the arc. They suggest that this feature may be a result of the acceleration process. In our example, however, this is not the case; the drop in the joule heating far exceeds the rise in the particle heating. This is due to the fact that while our densities are comparable to those measured by Evans et al. [1977], our fields are several times larger.

6. Conclusions and Discussion

This section will provide a summary and discussion of what we feel are the strongest and most important results. Those quantities which we feel are least subject to error are the densities (and thus conductivities) and the northward component of the electric field.

We emphasize first that we see no evidence at all of a density (or conductivity) enhancement equatorward of the auroral arc. As accurately as we can determine with the aid of the all-sky camera pictures and the antenna pointing direction (to perhaps a few kilometers), the enhancement of the density and the depletion of the electric field are coincident with the edge of the visible arc. We note that an enhancement of the conductivities equatorward of the arc has been postulated by some authors [Carlson and Kelley,

1977] in explaining the presence of an electric field in that region.

We found the northward field, which is calculated directly from the F region velocity measurements, to be exceptionally strong (>100 mV/m) in the region just equatorward of the arc. This field decreases to a value typical of the ambient convection field (≤40 mV/m) at a distance 100 km equatorward of the arc. The northward field within the arc also has a value roughly equal to the typical convection field. There is no apparent change in the magnitude of the northward field across the poleward boundary of the arc during the two clear passages of this boundary through the radar beam.

The major gradients in the poleward field are not located within the body of the arc. The increase in the field occurs entirely in the equatorward region. The decrease in the field appears to occur at the equatorward edge of the arc.

A further observation of interest is that the northward field retains its essential character over the nearly 1-hour period that observations were made. We continued to see effects qualitatively the same each time the equatorward edge of the arc was crossed, in spite of the fact that the appearance of the arc and the measured densities within the arc changed significantly. This observation suggests that the process producing the arc may, at times, be relatively stable. This observation will also be useful in planning and interpreting future radar arc experiments, since it is difficult to obtain good simultaneous measurements of both horizontal components of the fields and currents.

The results permit us to draw some conclusions regarding the source of the northward electric field, which has been a matter of some concern in earlier studies. Carlson and Kelley [1977], following the developments of Coroniti and Kennel [1972], suggested that the northward field they observed equatorward of an arc was the result of the polarization of a region of enhanced conductivity by an ambient westward field. We feel that such a process would not apply in the present case. Although we do have (questionable) evidence of a westward field in this region, we definitely do not see any enhancement of the conductivities. Furthermore, the mechanism of Coroniti and Kennel [1972] requires that with the westward field, the second spatial derivative of the density be positive for a polarization field

to result; our data provide no evidence for such a condition equatorward of the arc.

The study of de la Beaujardiere et al. [1977] does not directly address the source of the northward field but does conclude that the decrease of E_n within the arc may be due to a polarization effect of the Hall currents resulting from a westward field (this mechanism is outlined by Anderson and Vondrak [1975]). Again we feel that this mechanism is not applicable in the present case. The polarization field, which would have to be southward to cancel the strong northward field that we observe, would result from excess positive charge in the poleward boundary of the arc and excess negative charge in the equatorward boundary. If this were the case, and the magnitudes of the excess charges were equal, the polarization field outside the arc would be zero, and the measured field poleward of the arc should return to the equatorward value (or, at the least, show some increase). Our results, however, show relatively little change in the northward component of the field across the poleward edge of the arc; this indicates that the decrease of the field within the arc is not due to a polarization effect.

We conclude that the strong poleward field, and its decrease within the arc, are not effects produced directly by the enhanced density in the lower ionosphere. Furthermore, the field equatorward of the arc is considerably larger than the typical evening sunward convection field. These results suggest we should look elsewhere for the source of the northward field. Burch et al. [1976b], in the study of satellite data, suggest a possible alternative.

The latitudinal profile of the northward field that we observed bears a strong resemblance to fields that have been measured by satellites at altitudes below approximately 1000 km [e.g., Heppner, 1972; Gurnett, 1972; Burch et al., 1976a]. Satellites moving poleward in the evening sector frequently detect a northward field that displays a gradual increase followed by an abrupt decrease. This feature typically spans several hundred kilometers [Heppner, 1972; Gurnett, 1972]. Similar enhancements on the scale of only a hundred kilometers or less have also been seen [Burch et al., 1976a]. Burch et al. [1976a] also found that the decrease in the electric field is accompanied by precipitating electrons (inverted v's). The precipitating electrons presumably produce auroral arcs.

This gradual enhancement of the field, followed by a more rapid decrease and the presence of auroral particles, is precisely what we have observed with the radar. In their study of shear flow reversals, Burch et al. [1976b] suggest that the northward field observed at satellite altitudes (≈280 km) may have been mapped down from the region that accelerates the auroral particles. Although they were specifically discussing cases where the northward field showed a pronounced reversal, and not merely an abrupt decrease, we feel that many of the essential features of our case are similar and that the same reasoning may apply. We note, however, that our case is much less symmetric than the events Burch et al. [1976b] discuss and that this may imply a notably different structure to the field associated with the acceleration region.

A model proposed by Vondrak [1975] suggests an alternate explanation. This model assumes that an upward current produces an enhanced particle density and a net space charge only within the body of the arc. If it is further postulated that the return current can flow only on the equatorward side of the arc, the resulting electric field and current profiles are similar to those in our data. A more thorough investigation of these possibilities should await the accumulation of more data.

We remind the reader that this arc appears to be somewhat unique among those studied thus far and that our conclusions may not apply to other cases; the possibility also exists, however, that due to the existence of the exceptionally strong field, we have a better opportunity to observe the features of the arc uncontaminated by extraneous effects. In any case we heartily recommend that future studies of arcs take care to determine, if possible, the fields not only immediately adjacent to the arcs but also extending to at least 100 km either side of the arcs. These observations should be of help in correctly separating the ambient from the true arc-associated fields.

Aknowledgments. This work was performed under National Science Foundation grant ATM76-17334. The Chatanika staff of SRI International deserve special thanks for their patience in assisting our operations. We would also like to thank R. R. Vondrak and the reviewers for their helpful comments.

The Editor thanks O. de la Beaujardiere and R. A. Greenwald for their assistance in evaluating this paper.

References

Akasofu, S.-I., Physics of Magnetospheric Substorms, D. Reidel, Hingham, Mass., 1977.

Anderson, H. R., and R. R. Vondrak, Observations of Birkeland currents at auroral latitudes, Rev. Geophys. Space Phys., 13, 243, 1975.

Arnoldy, R. L., The relationship between field-aligned current, carried by supra-thermal electrons, and the auroral arc, Geophys. Res. Lett., 4, 407, 1977.

Banks, P. M., Observations of joule and particle heating in the auroral zone, J. Atmos. Terr. Phys., 39, 179, 1977.

Baron, M. J., The Chatanika radar system, in Radar Probing of the Auroral Plasma, edited by A. Brekke, Universitetsforlaget, Oslo, 1977.

Brekke, A., J. R. Doupnik, and P. M. Banks, A preliminary study of the neutral wind in the auroral E region, J. Geophys. Res., 78, 8235, 1973.

Brekke, A., J. R. Doupnik, and P. M. Banks, Observations of neutral winds in the auroral E region during the magnetospheric storm of August 3-9, 1972, J. Geophys. Res., 79, 2448, 1974a.

Brekke, A., J. R. Doupnik, and P. M. Banks, Incoherent scatter measurements of E region conductivities and currents in the auroral zone, J. Geophys. Res., 79, 3773, 1974b.

Burch, J. L., S. A. Fields, W. B. Hanson, R. A. Heelis, R. A. Hoffman, and R. W. Janetzke, Characteristics of auroral electron acceleration regions observed by Atmosphere Explorer C, J. Geophys. Res., 81, 2223, 1976a.

Burch, J. L., W. Lennartsson, W. B. Hanson, R. A. Heelis, J. H. Hoffman, and R. A. Hoffman, Properties of spike-like shear flow reversals observed in the auroral plasma by Atmosphere Explorer C, J. Geophys. Res., 81, 3886, 1976b.

Carlson, C. W., and M. C. Kelley, Observation and interpretation of particle and electric field measurements inside and adjacent to an active auroral arc, J. Geophys. Res., 82, 2349, 1977.

Casserly, R. T., Jr., and P. A. Cloutier, Rocket-based magnetic observations of auroral Birkeland currents associated with a structured auroral arc, J. Geophys. Res., 80, 2165-2168, 1975.

Coroniti, F. V., and C. F. Kennel, Polarization of the auroral electrojet, J. Geophys. Res., 77, 2835, 1972.

de la Beaujardiere, O., R. Vondark, and M. Baron, Radar observations of electric fields and currents associated with auroral arcs, J. Geophys. Res., 82, 5051, 1977.

Doupnik, J. R., A. Brekke, and P. M. Banks, Incoherent scatter radar observations during three sudden commencements and a Pc 5 event on August 4, 1972, J. Geophys. Res., 82, 499, 1977.

Evans. D. S., N. C. Maynard, T. Trøim, T. Jacobsen, and A. Egeland, Auroral vector electric field and particle comparisons, 2, Electrodynamics of an arc, J. Geophys. Res., 82, 2235, 1977.

Gurnett, D. A., Electric field and plasma operations in the magnetosphere, in Critical Problems of Magnetospheric Physics, edited by E. R. Dyer, 123, National Academy of Sciences, Washington, D. C., 1972.

Heppner, J. P., Electric fields in the magnetosphere, in Critical Problems of Magnetospheric Physics, edited by E. R. Dyer, p. 107, National Academy of Sciences, Washington, D. C., 1972.

Kelley, M. C., and C. W. Carlson, Observations of intense velocity shear and associated electrostatic waves near an auroral arc, J. Geophys. Res., 82, 2343, 1977.

Leadabrand, R. L., M. J. Baron, J. Petriceks, and H. F. Bates, Chatanika, Alaska, auroral zone incoherent scatter facility, Radio Sci., 7, 747, 1972.

Maynard, N. C., D. S. Evans, B. Maehlun, and A. Egeland, Auroral vector electric field and particle comparisons, 1, Premidnight convection topology, J. Geophys. Res., 82, 2227, 1977.

Rino, C. L., A. Brekke, and M. J. Baron, High-resolution auroral zone E region neutral wind and current measurements by incoherent scatter radar, J. Geophys. Res., 82, 2295, 1977.

Vondrak, R. F., Model of Birkeland currents associated with an auroral arc, J. Geophys. Res., 80, 4011-4014, 1975.

(Received January 4, 1979;
revised October 22, 1979;
accepted October 23, 1979.)

TABLE 1. Antenna Positions, January 29, 1977

Time, UT	Magnetic Azimuth, deg	Elevation, deg
0918:12-0921:13	180	76.5
0921:29-0924:30	111	58
0924:41-0927:42	104	50
0927:51-0930:52	107	54.6
0931:03-0934:04	114	61
0934:13-0937:13	118	64
0937:24-0940:24	110	57.9
0940:36-0943:37	104	50
0943:46-0946:47	107	54.6
0946:58-0949:54	114	61
0950:16-0951:17	98	37.5
0951:38-0954:39	180	76.5
0954:55-0957:56	111	57.9
0958:07-1001:08	104	50
1001:18-1004:19	107	54.6
1004:30-1007:30	114	61
1007:39-1010:40	118	64
1013:14-1018:13	120-150*	60
1018:14-1023:11	150-120	60
1024:12-1032:29	120-170	60
1032:29-1040:45	170-120	60

*Scan.

Fig. 1. DMSP photo taken at 0947 UT, January 29, 1977. Chatanika is located beneath the equatorward portion of the arc just off the frame to the right.

Fig. 2. All-sky camera photographs (negative) taken from Chatanika on January 29, 1977. The black and white circles denote the position of the radar beam. The moon is in the southwest corner, and its reflection in the lens can be seen near the top of the communications antenna pole. All times are UT.

Fig. 3. (Top) Electron density integrated along the line of sight from 80- to 170-km altitude. Measurements are from 15-s integrations of the radar signal. Breaks in the data occur when the antenna positioning mode is changed. The horizontal bars indicate roughly when the radar beam is within the arc. 'E' and 'P' refer to when the beam is equatorward and poleward, respectively, of the arc. The small horizontal tics at 1.6×10^{12} cm^{-2} indicate the equatorward (Figure 9) and poleward (Figure 10) passages of the edges of the arc through the radar beam. (Bottom) F region (solid line) and E region (dashed line) line of sight velocities. Positive velocities indicate flow toward magnetic west.

Fig. 4. Density profiles derived from 3-minute averages of the radar data. Profiles were taken (a) ~100 km equatorward of the arc, (b) immediately equatorward of the arc, and (c) within the arc. The three profiles are superimposed upon one another in (d). The densities are plotted only to the altitude where they become dominated by noise.

Fig. 5. Calculated northward (solid line) and eastward (dashed line) electric fields.

Fig. 6a. Conductivities integrated from 80- to 170-km altitude. The Hall conductivity (solid line) is nearly always greater than the Pederson conductivity (dashed line).

Fig. 6b. Calculated height-integrated northward (solid line) and eastward (dashed line) currents.

Fig. 7. H and Z traces from the Poker Flat magnetometer. Positive is upward for both traces. The dashed lines represent quiet time levels.

Fig. 8. Joule (solid line) and particle (dashed line) heating rates integrated from 80 to 170 km.

Fig. 9. Four superimposed passes of the radar beam through the equatorward edge of the arc. The plots have been aligned at points where the height-integrated density passes through 1.6×10^{16} cm^{-2}. The horizontal axis is actually time. The distance scale is derived from all-sky camera photos and is only approximate. The times of the passages are shown in Figure 3.

Fig. 10. Two superimposed passages of the radar beam through the poleward edge of the arc. The plots have been aligned at the points where the height-integrated density passes through 1.6×10^{16} cm^{-2}. The times of the passages are shown in Figure 3.

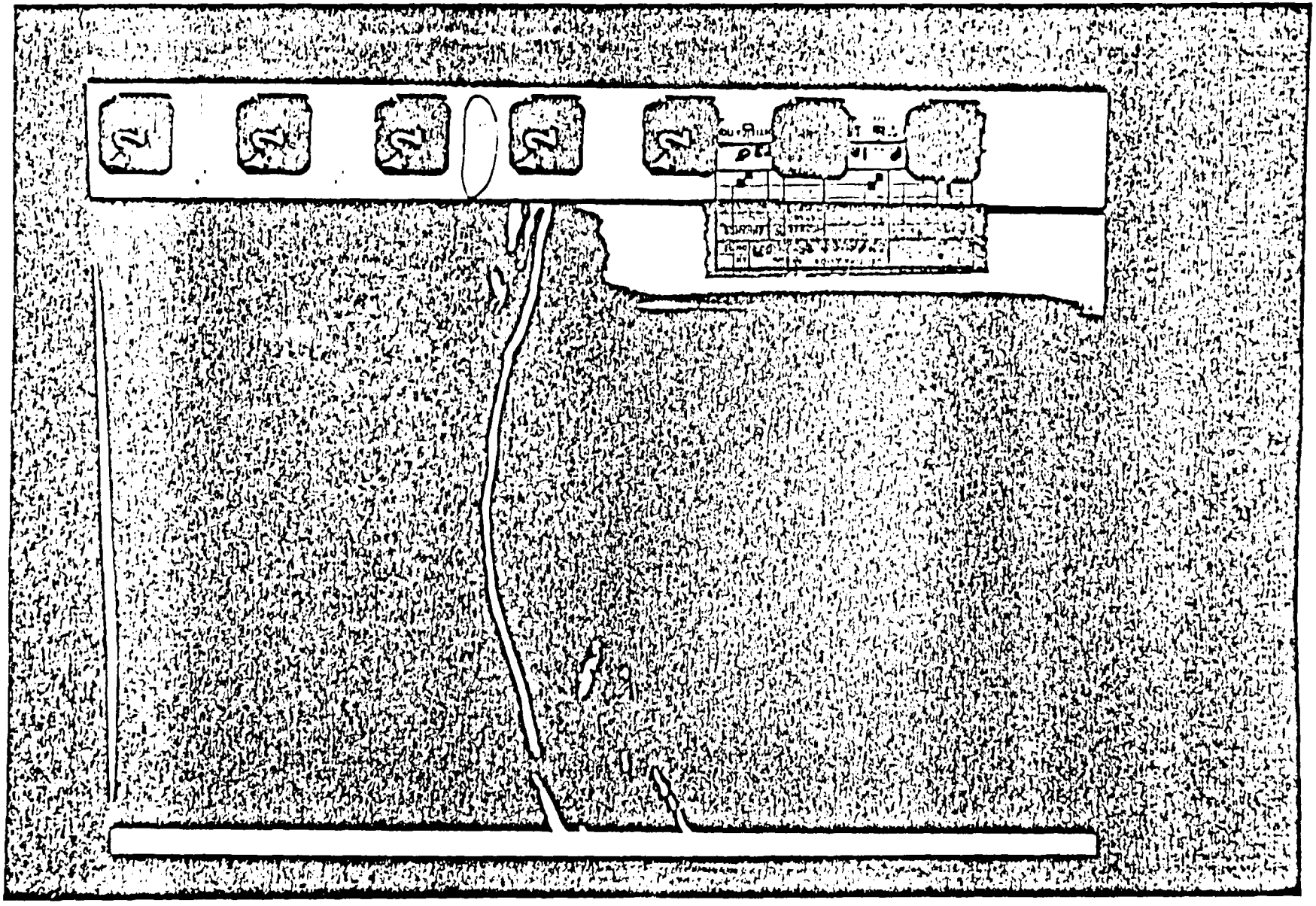

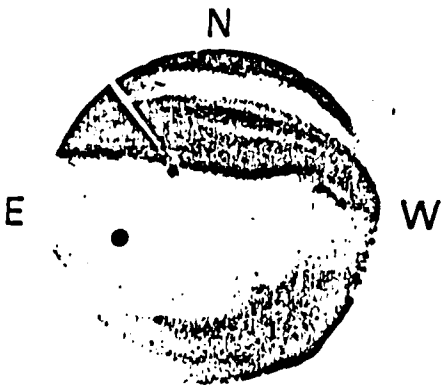

0937

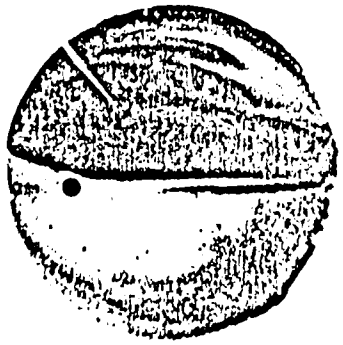

0941

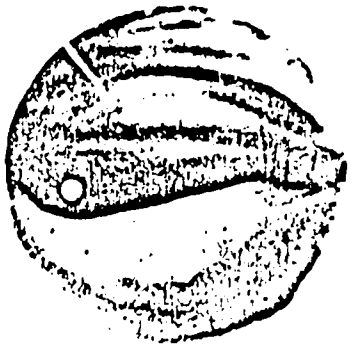

0943

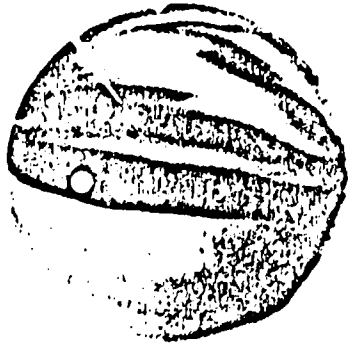

0945

0947

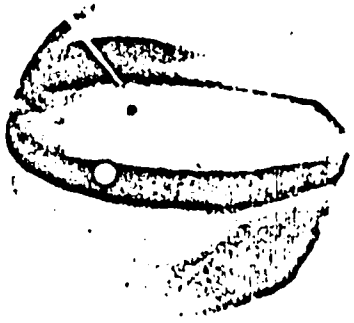

0950

CHAT 29 JAN. 77

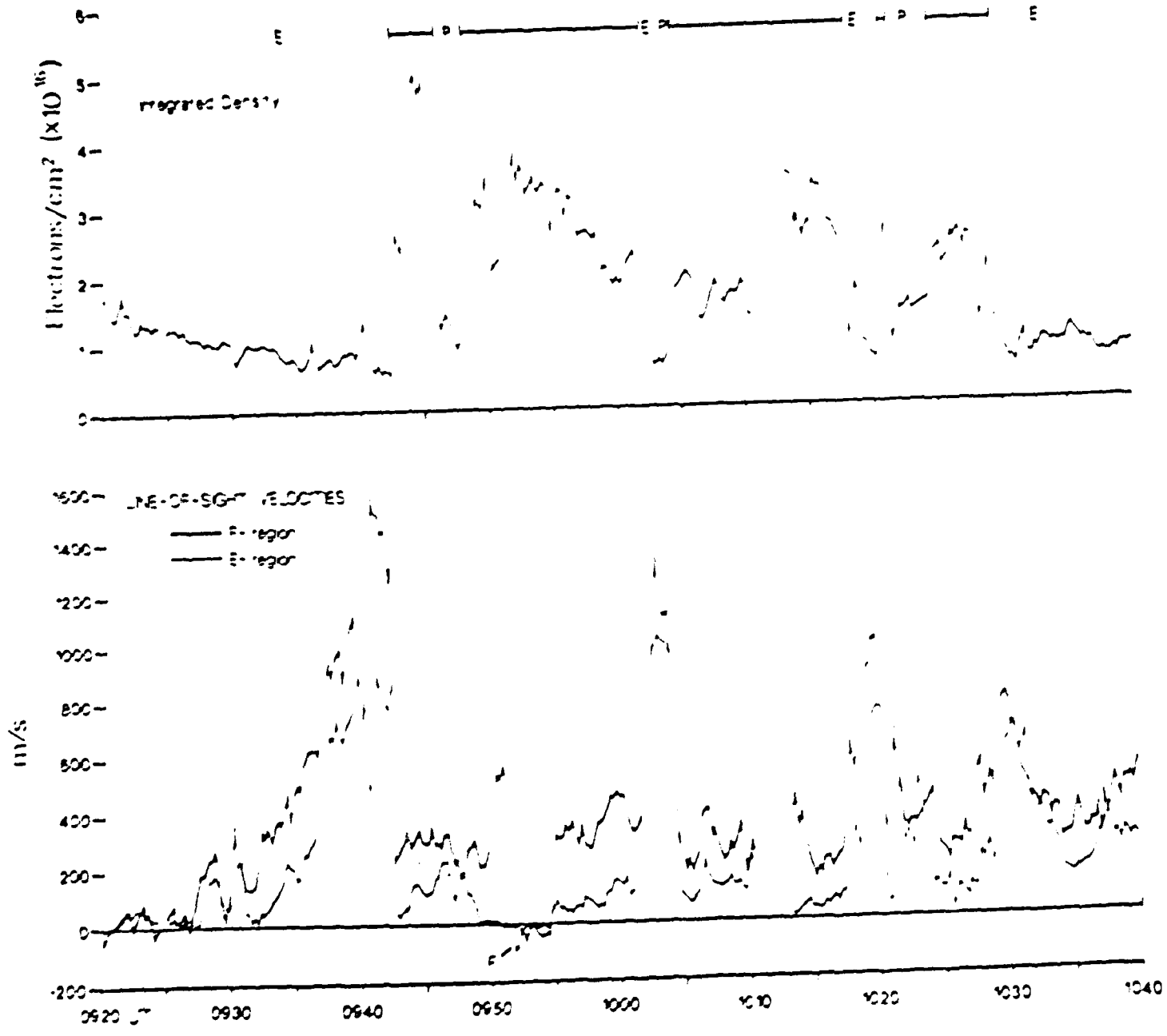
E
P
E
P
E
P
E
Integrated Density
Electrons/cm² (x10¹⁶)
6
5
4
3
2
1
0
LINE-OF-SIGHT VELOCITIES
E-region
E-region
m/s
1600
1400
1200
1000
800
600
400
200
0
-200
0920
0930
0940
0950
1000
1010
1020
1030
1040

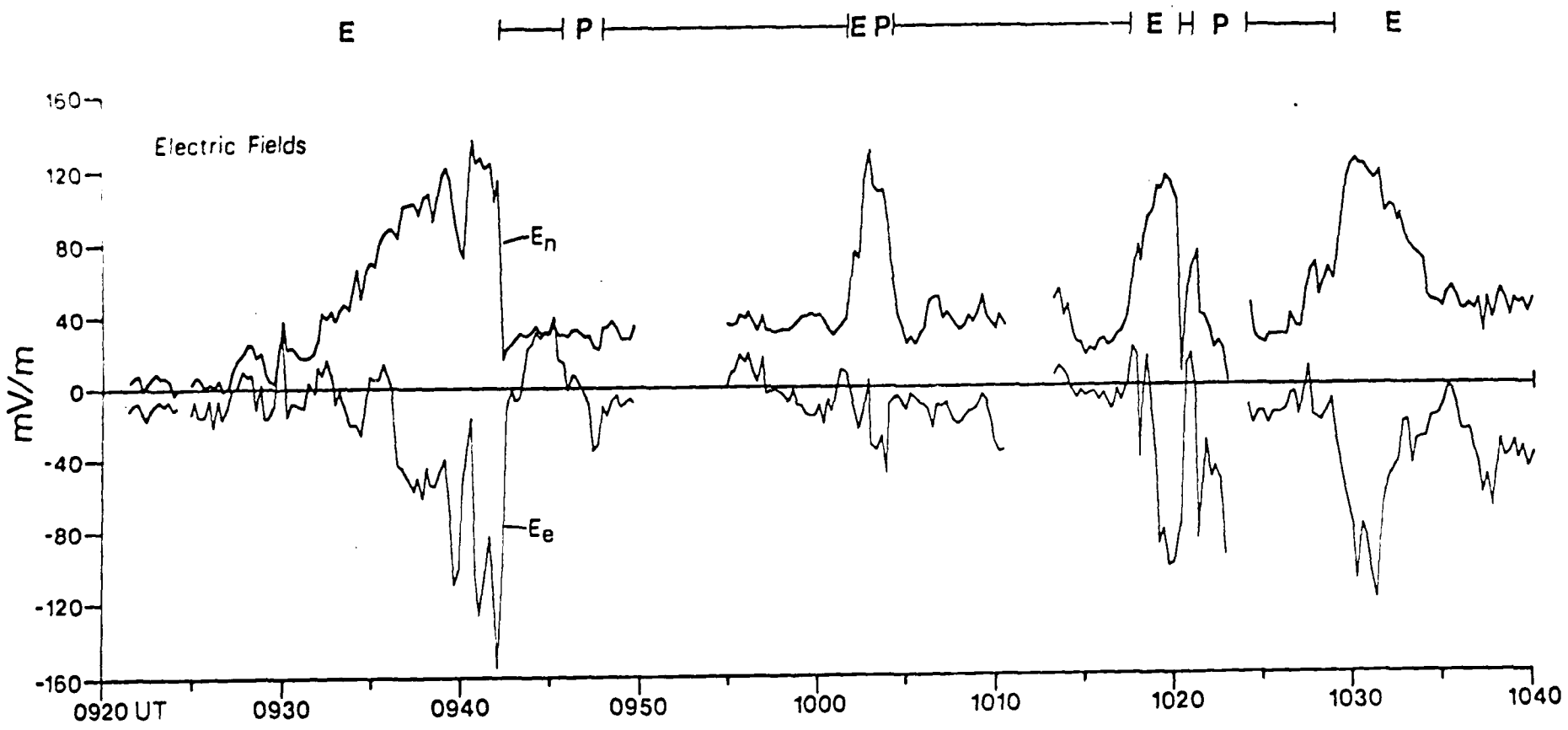
E
P
E P
E H P
E
Electric Fields
160
120
80
40
0
-40
-80
-120
-160
mV/m
E_n
E_e
0920 UT
0930
0940
0950
1000
1010
1020
1030
1040

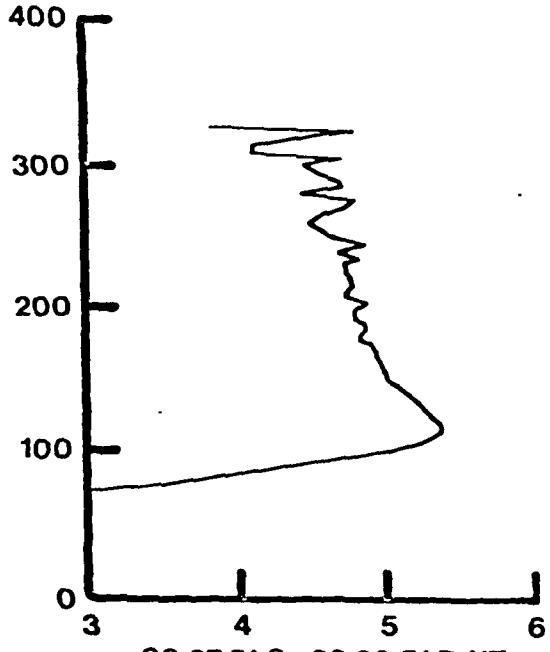

09 27 51.8 - 09 30 51.7 UT

(a)

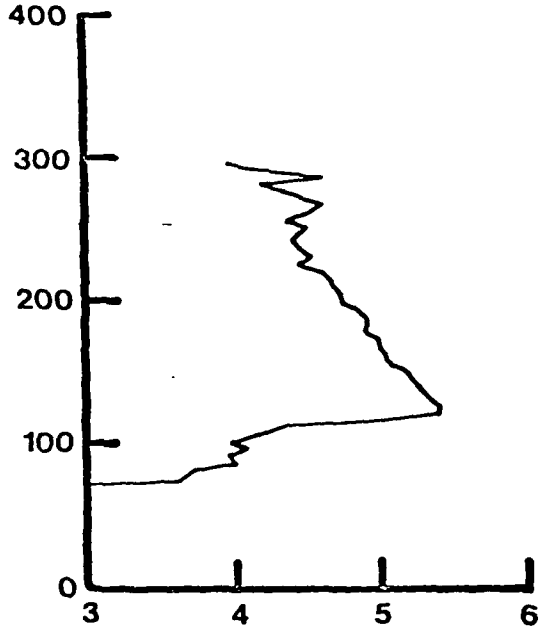

09 37 24.1 - 09 40 24.0 UT

(b)

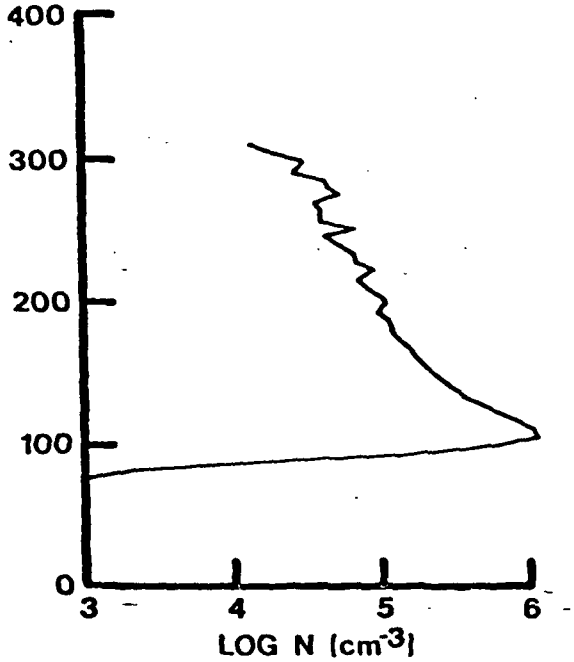

09 51 38.9 - 09 54 38.8 UT

(c)

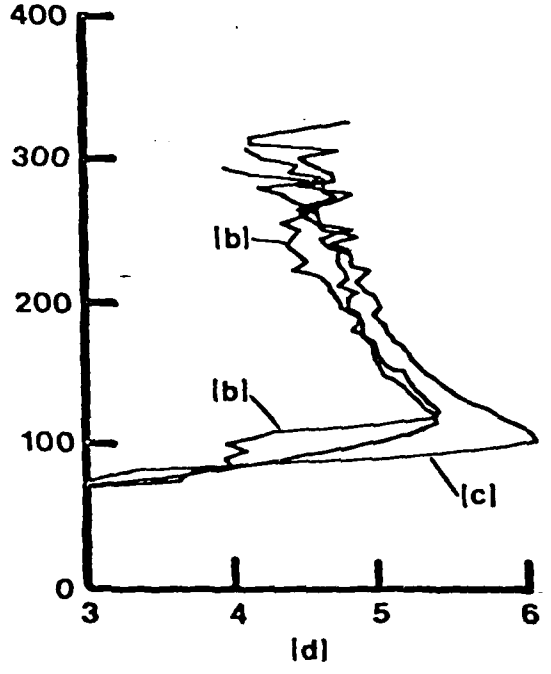

(d)

CHATANIKA
29 JAN, 1977

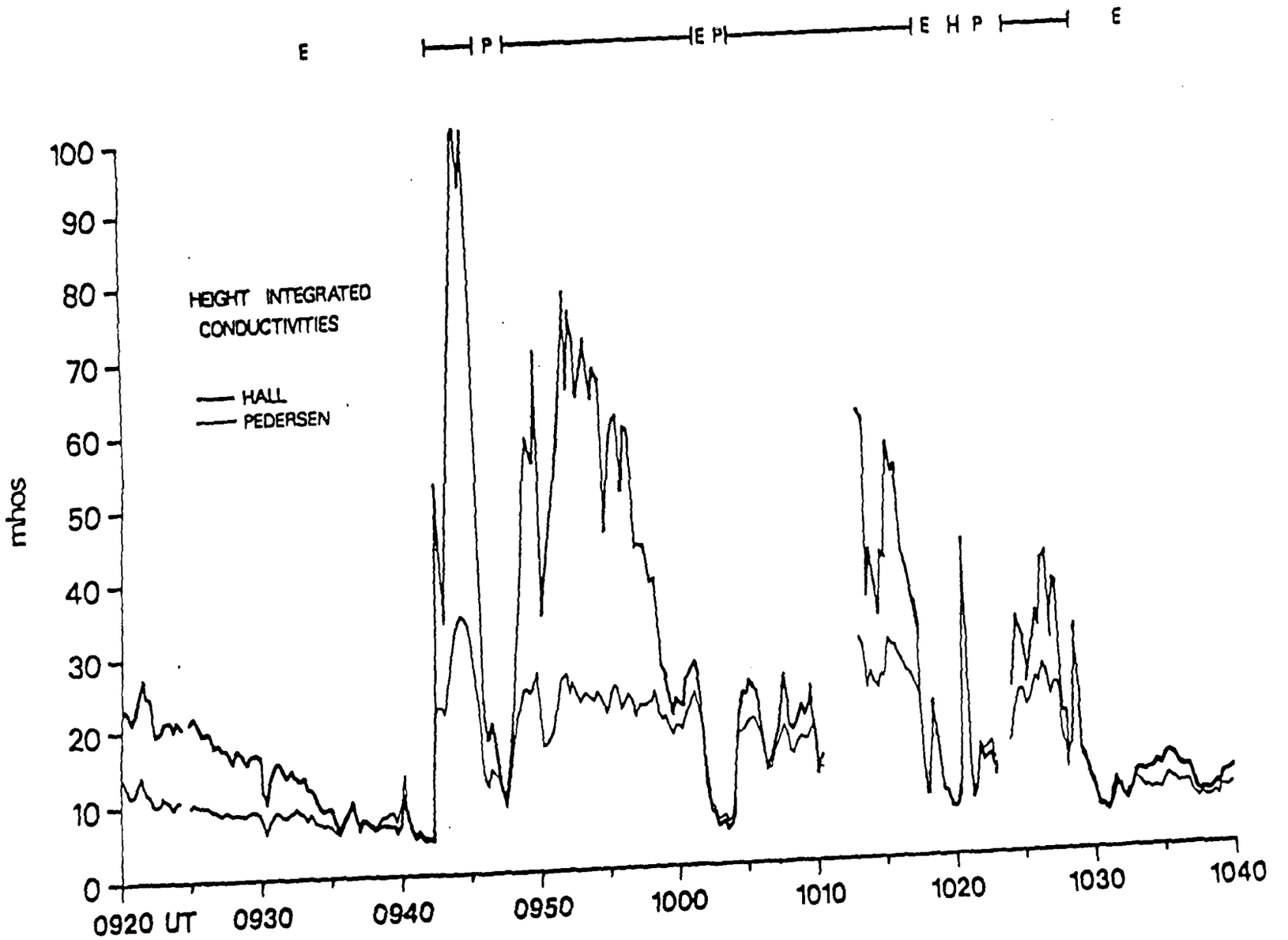
E
P
E P
E H P
E
HEIGHT INTEGRATED
CONDUCTIVITIES
HALL
PEDERSEN
mhos
100
90
80
70
60
50
40
30
20
10
0
0920 UT
0930
0940
0950
1000
1010
1020
1030
1040

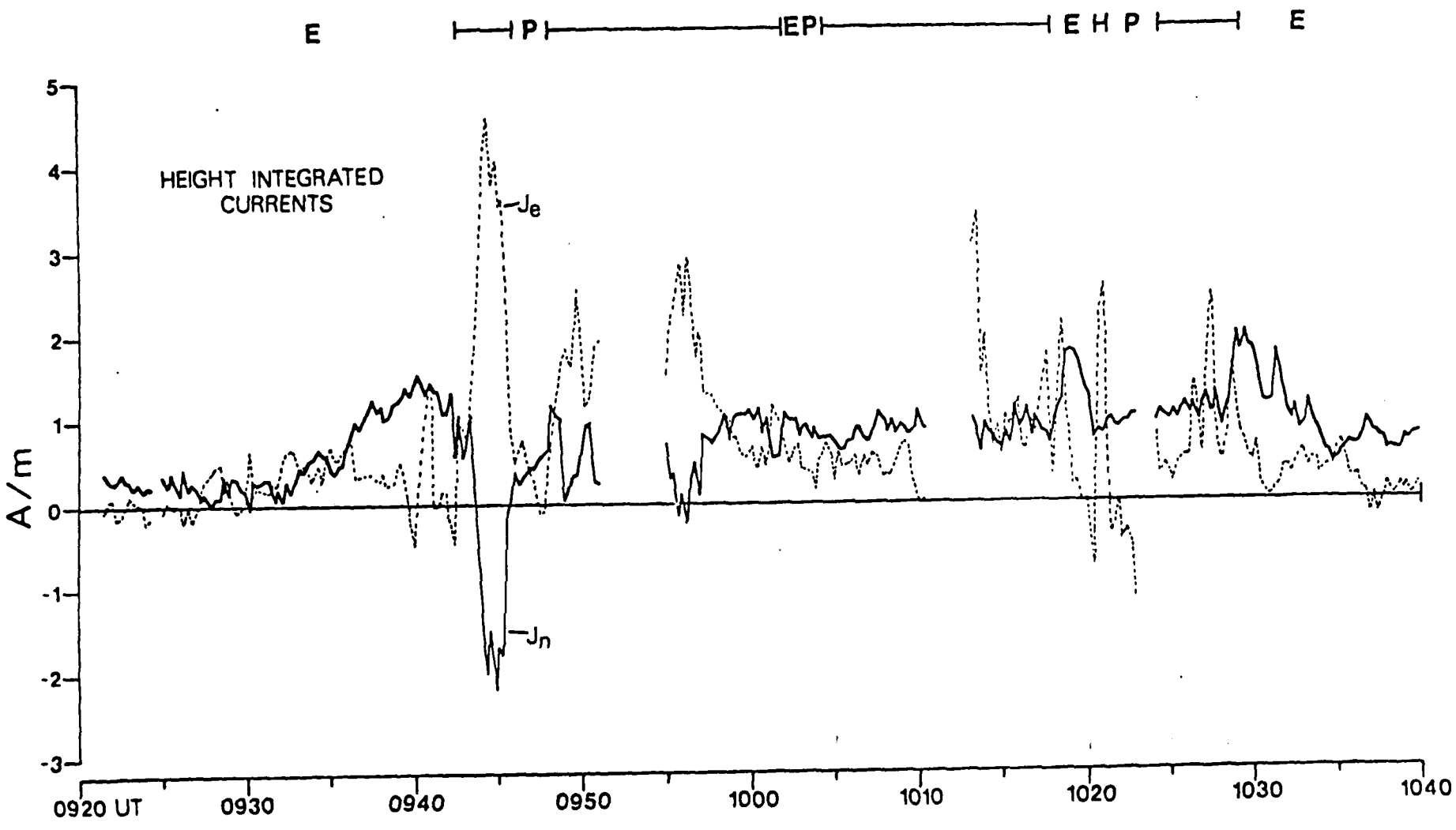
E
P
EP
E H P
E
HEIGHT INTEGRATED
CURRENTS
J_e
J_n
A/m
5
4
3
2
1
0
-1
-2
-3
0920 UT
0930
0940
0950
1000
1010
1020
1030
1040

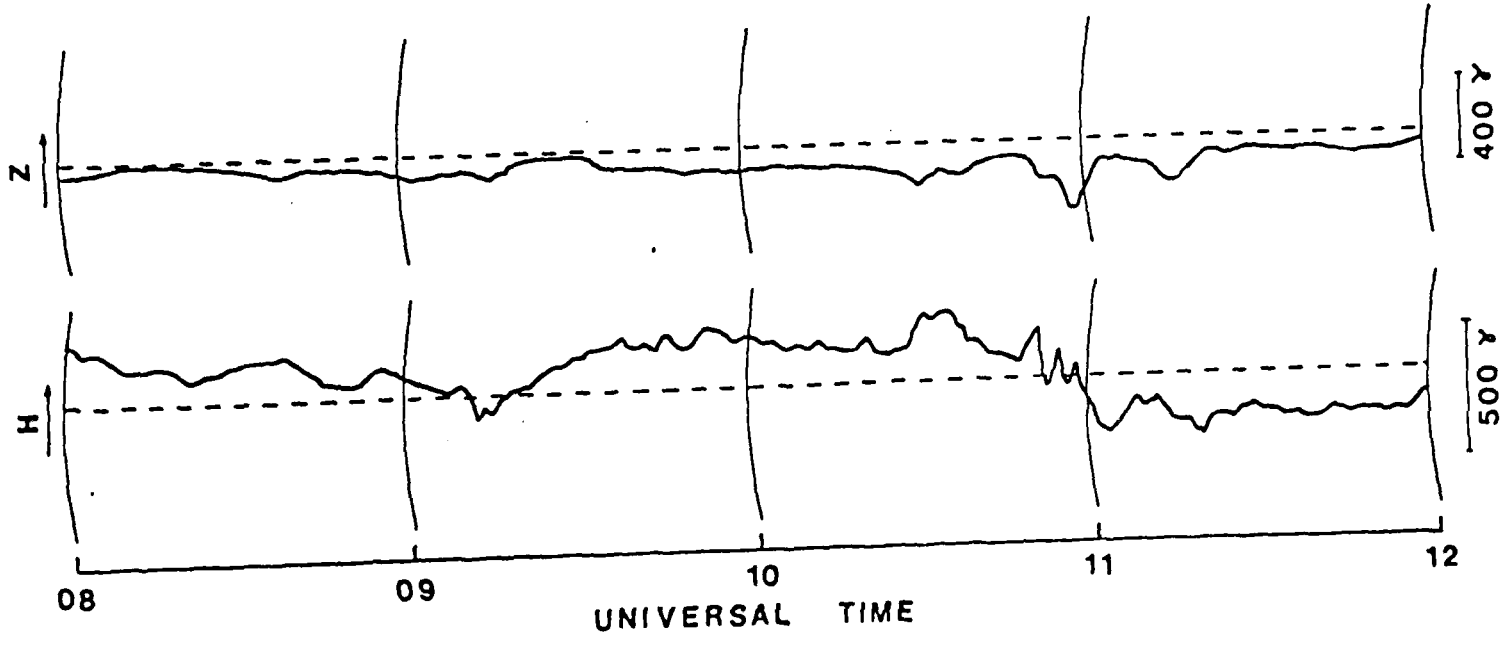
Z
400 γ
H
500 γ
08
09
10
11
12
UNIVERSAL TIME

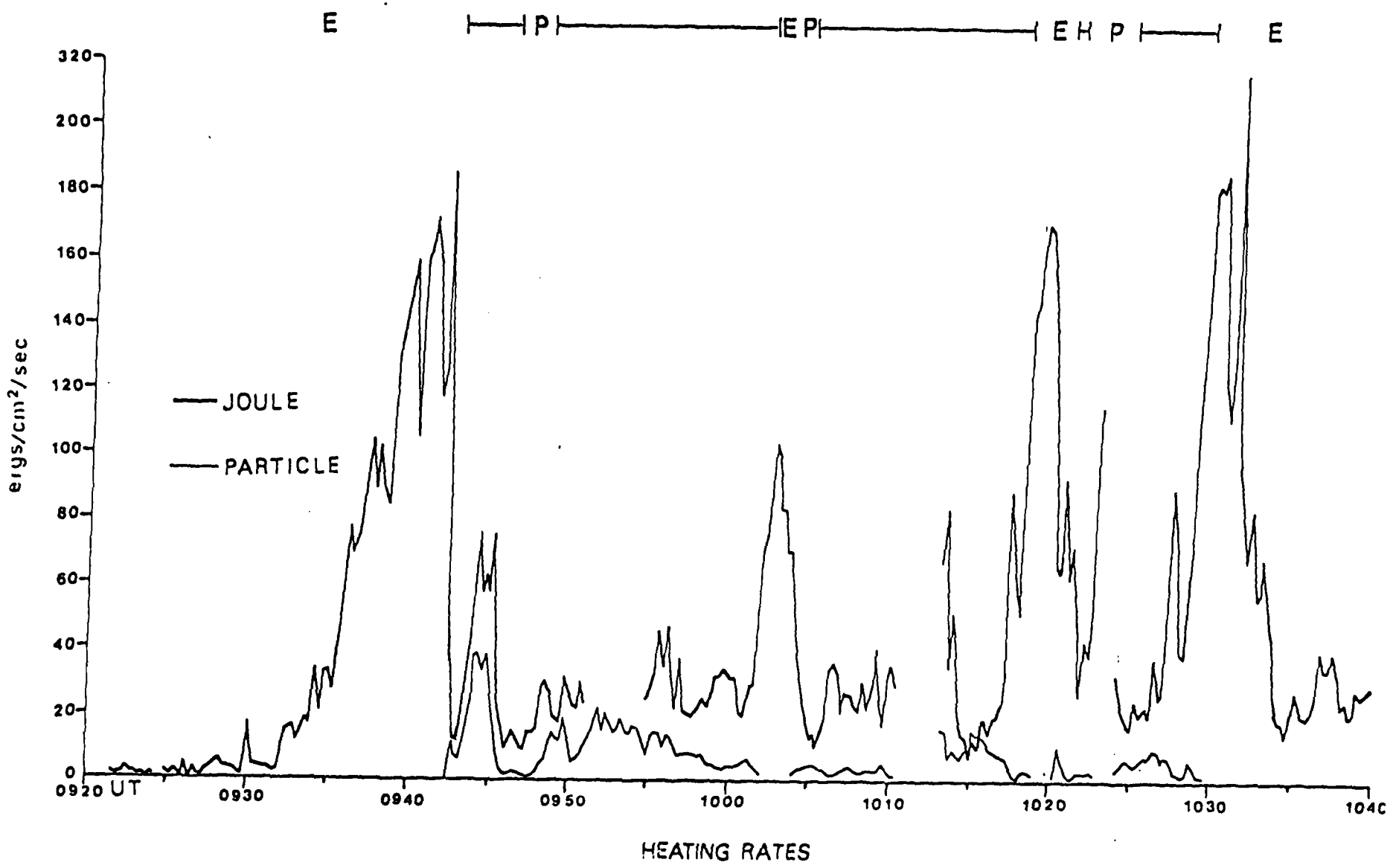
E
P
E P
E H P
E
320
200
180
160
140
120
100
80
60
40
20
0
ergs/cm²/sec
JOULE
PARTICLE
0920 UT
0930
0940
0950
1000
1010
1020
1030
1040
HEATING RATES

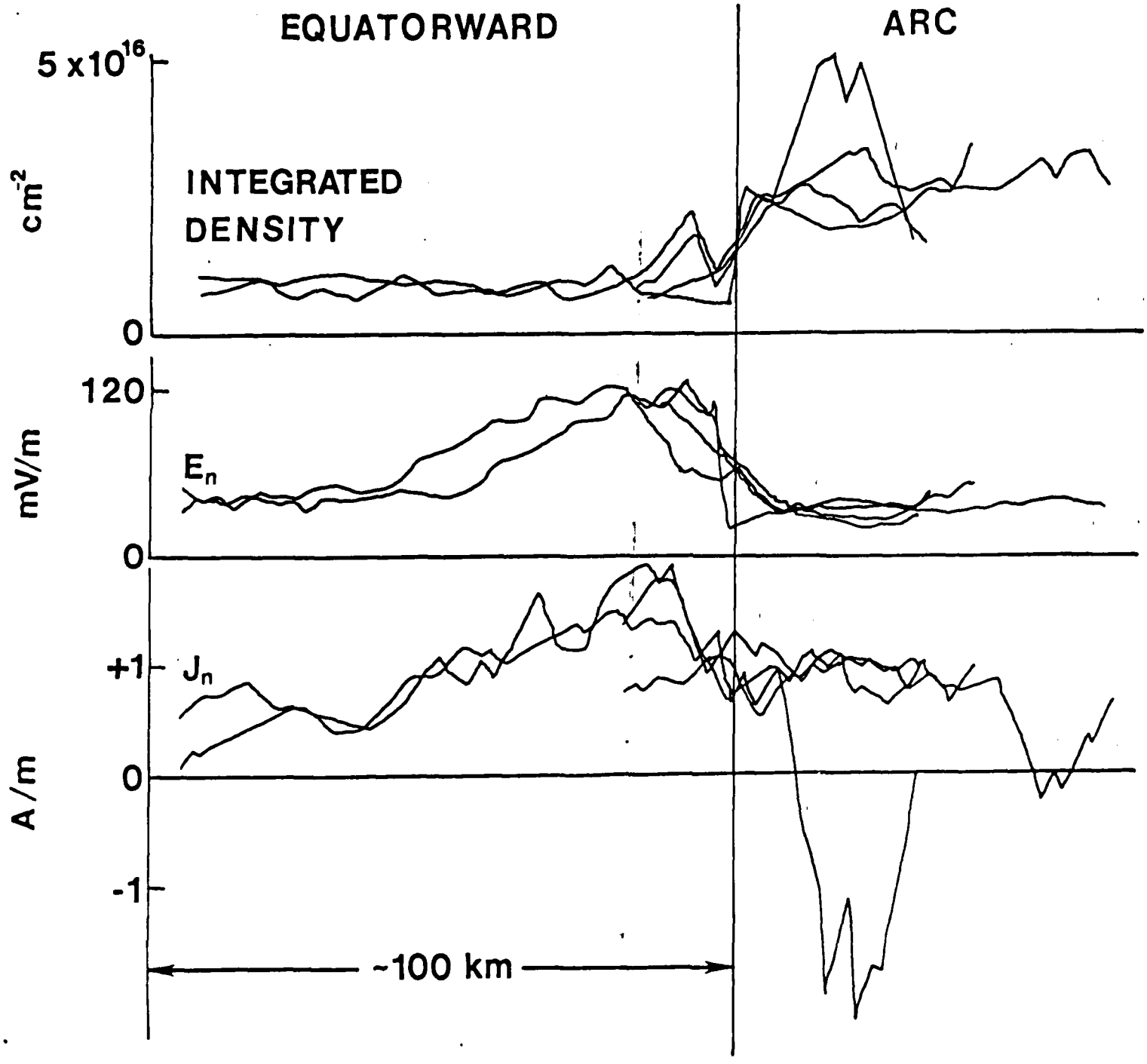
EQUATORWARD
ARC
5 x10^16
cm^-2
INTEGRATED
DENSITY
0
120
mV/m
E_n
0
+1
J_n
A/m
0
-1
~100 km

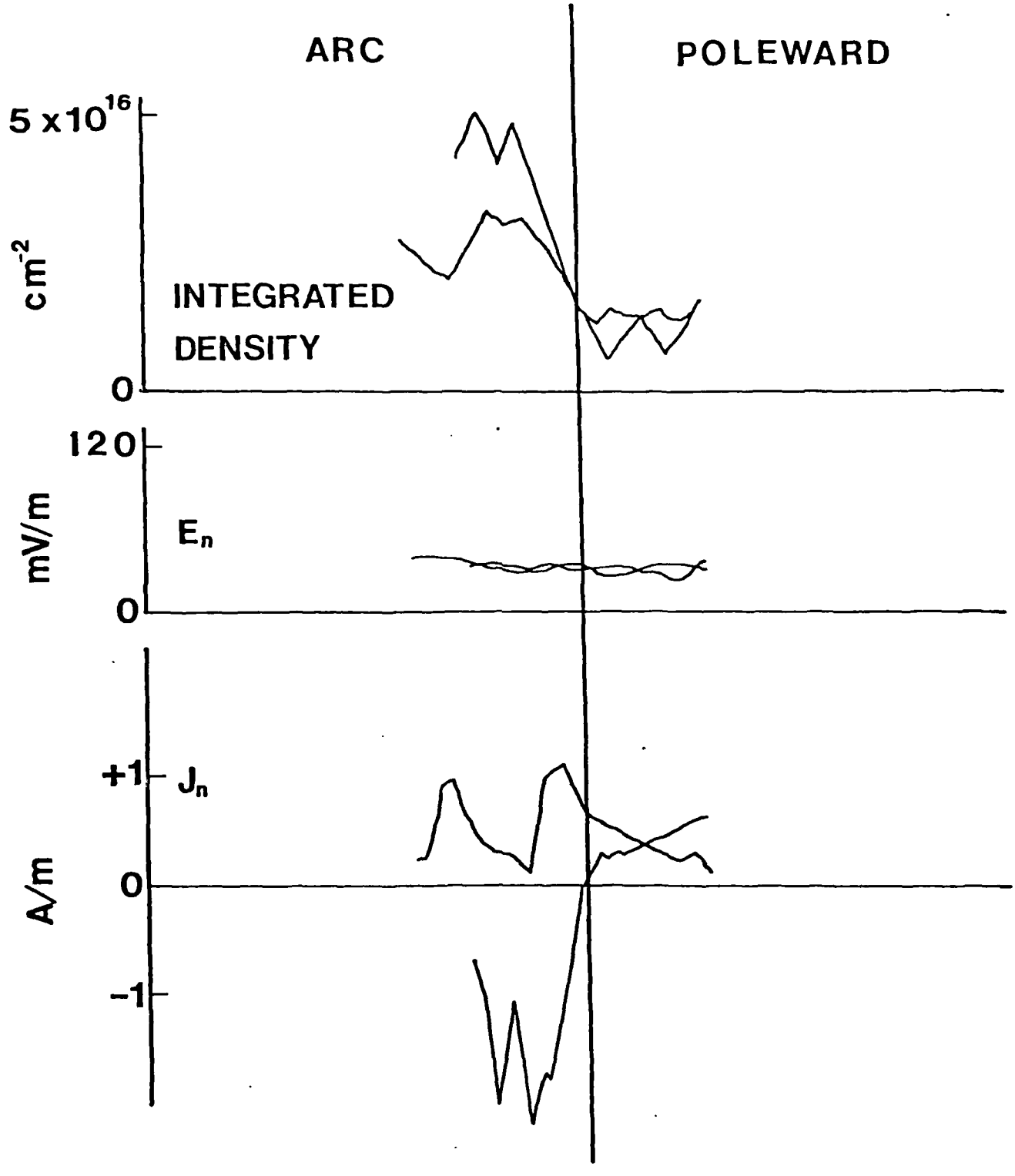
ARC
POLEWARD
5 x 10^16
cm^-2
INTEGRATED
DENSITY
0
120
mV/m
E_n
0
+1
J_n
A/m
0
-1

Revised

9/79

High Latitude Convection: Comparison of a Simple Model with Incoherent Scatter Observations

J.J. Sojka, J.C. Foster, W.J. Raitt, R.W. Schunk
and J.R. Doupnik

Center for Atmospheric and Space Sciences
Utah State University, UMC 41
Logan, Utah 84322

Submitted to:
J. Geophys. Res.
June, 1979

ABSTRACT

We have compared a simple model of plasma convection at high latitudes with data obtained from simultaneous measurements made by the incoherent scatter facilities at Chatanika, Alaska and Millstone Hill, Massachusetts in June 1978 during moderately disturbed conditions. The measured horizontal plasma drift velocities were averaged for four days to emphasize gross features of the convection pattern and reduce the effects of substorms.

The convection model includes the offset of 11.5^{o} between the geographic and geomagnetic poles, the tendency of plasma to corotate about the geographic pole, and a constant dawn/dusk magnetospheric electric field mapped to a circle about a center offset by 5^{o} in the anti-sunward direction from the magnetic pole. The radius of the circle corresponds to 17^{o} of latitude and the electric potentials are aligned parallel to the noon/midnight meridian within the circle. Equatorward of the circle the potential diminishes radially and varies inversely as the fourth power of sine magnetic co-latitude. A consequence of these two offsets and the sunward alignment of the magnetospheric electric field is that our model predicts different diurnal convection patterns when viewed at different longitudes in the geographic frame.

The concurrently observed diurnal distributions of horizontal plasma convection velocities are different for Chatanika and Millstone Hill even though the measurements cover approximately the same range of magnetic latitudes. We find there is good agreement between our simple model and the gross features of these two diurnal patterns.

1. INTRODUCTION

In an earlier paper (Sojka et al., 1979) we presented a simple model for the dawn/dusk magnetospheric electric field mapped to the ionosphere, and we discussed the resulting effect on the flow velocities of ionospheric plasma at high latitudes. We found that the displacement between the geographic and geomagnetic poles significantly affected the competition between the co-rotation flow of the plasma and the convective flow due to the magnetospheric electric field. In a magnetic quasi-inertial frame with the z-axis parallel to the dipole axis and the sun lying in the x-z plane, the flow was shown to be Universal Time (U.T.) independent for a constant magnetospheric electric field. However, the flow pattern becomes U.T. dependent when viewed in a geographic inertial frame of reference because of the rotation of the geomagnetic pole about the geographic pole.

In this study we have endeavored to improve and substantiate our model by comparing model predictions of plasma flow patterns with observations by the incoherent scatter radar technique. Of particular interest are differences of plasma flow predicted by the model at different longitudes but otherwise at the same invariant latitude and local time. Experimental data employed were obtained by the Chatanika, Alaska and Millstone Hill, Massachusetts incoherent radar facilities during concurrent operations over four days in June 1978.

2. Experiment Description

Both incoherent scatter radars were operated extensively during the same four day period to measure the ion drift velocity vector in the F-region over the range of invariant latitudes 55^{o} to 76^{o} along their respective geomagnetic meridians. Chatanika, located near Fairbanks, Alaska, has a magnetic meridian pointing 29^{o} east of geographic north and sampled the region 56^{o} to 74^{o} invariant latitude (55^{o} to 73^{o} geographic). Millstone Hill radar has a magnetic

meridian pointing 3^{o} west of geographic north and sampled the region 55^{o} to 72^{o} invariant latitude (44^{o}-58^{o} geographic). Five hours of local time separate the stations.

Both experiments utilized their very narrow beam antennas to sample the ionosphere at a succession of paired positions near their magnetic meridians. Many observations were obtained in each position by sampling at different ranges. The new 45 m steerable antenna (Evans et al., 1978) was used at Millstone Hill with excellent effect.

The local time separation between the individual samples entering into a velocity vector calculation was less than one hour for Chatanika and two hours for Millstone Hill. Maximum separation naturally occurs at the most extreme ranges and was minimized consistent with maintaining low overall statistical uncertainty of the predominant east-west flow velocity.

A set of velocity vectors could be obtained with a pair of antenna positions in about 5 minutes or less, and the same region was sampled again at about 30 minute intervals. Both Chatanika and Millstone Hill radar data were analyzed at USU using essentially the same methods. It is clearly impractical here to present error bars on the velocity vectors, but perhaps the ensemble of vectors shown will suffice. Unacceptable data were discarded by statistical signal criteria before the vectors were computed, but noisy data are evident at the extreme ranges (to the far north and south for Chatanika, and just to the far north for Millstone Hill).

Observational Data

The upper panels of figures 1 and 2 show the ion drift velocities obtained respectively from Chatanika and Millstone Hill for four days of experiments. For the purposes of this paper the detailed measurements have been sorted into half - hour U.T. bins and have also been averaged over the set of four days.

Further, although the data are shown in geographic coordinates to facilitate comparison with the models, each station's measurements covered nearly the same invariant latitudes. A vector is plotted as a dot at the central point of observation with a line indicating strength and direction.

Although the temptation is strong to consider these data as a 'snap shot' of the entire auroral convection pattern they are really scans over the same invariant latitudes accumulated over a 24 hour period. The overall patterns nevertheless are those commonly encountered in many similar experiments. Substorms occurred which produced strong reorientations of the flow lasting for 30 minutes to over an hour and are impossible to remove from the data set simply by averaging.

3. Comparison of Model Predictions With Observations

Development of the Convection Model

The initial objective of this study was to compare the simple plasma flow model of Sojka et al. (1979) with experimental plasma flow observations. The model assumes that the ionospheric plasma tends to corotate about the geographic pole, and that the magnetospheric electric field maps into the ionosphere about the geomagnetic pole. This electric field is represented by a uniform dawn-dusk electric field within a circle bounded by 75^{o} geomagnetic latitude. The magnetic field model used is that of a dipole field. Equatorward of this circle the electric potential diminishes meridionally and inversely as the fourth power of the sine of magnetic co-latitude. The consequence of an offset between the geographic and geomagnetic poles is to introduce very marked universal time variations which are apparent when observing the plasma flow in the geographic frame at different longitudes yet at the same local time and magnetic latitude.

The predicted plasma flow pattern for Chatanika is shown in Figure 3 for this simple convection model. The display format was chosen to match that of

the data (figure 1, upper panel). This model reproduces only the gross characteristics of the observed ion drift pattern; namely, the westward and eastward flow directions in the local evening and morning sectors (the zonal flow pattern) and the west south-east reversal around midnight. The most obvious feature of the experimental data is the movement of the convection field to low latitudes at night and its retreat to high latitudes in the day, a feature which is absent from the model predictions shown in figure 3. Also the model predictions are much more symmetric in local time than are the observations. In particular, the Chatanika data show a region of non zonal flow moving to a lowest latitude of 68^{o} near local midnight and poleward out of the range of the radar near local noon. This region is not predicted by the model calculations shown in figure 3. This last feature is indicative of a boundary in the drift pattern moving towards Chatanika around 10 UT and away again around 18 UT.

In order to include such a feature in the model the center of the circle defining the magnetospheric electric field boundary was shifted antisunward along the magnetic midnight meridian by 5^{o}. Motivation for this offset can be found by looking at the nearly circular quiet time inner boundary of the Feldstein oval (Feldstein, 1963), DMSP low light observations (Meng et al., 1977) and particle observations (Meng, 1979). A second, minor, adjustment is that the radius of the electric field circle is increased from the 15^{o} of the initial model to 17^{o}.

For comparison with the radar data of figure 1, a cross tail potential of 90 kV was selected so that the model predictions and observations would agree with regard to the magnitude of the drift velocity vectors in the afternoon sector. This potential corresponds to moderately active conditions and is consistent with the activity at the time the measurements were made.

Comparison with Observations

Using the improved model described in the previous subsection, the ion drift patterns for both the Chatanika and Millstone Hill sites have been calculated; these are shown in figures 1 and 2 (lower panels), respectively. The predictions of the improved model are seen to be in good qualitative agreement with the observations.

At Chatanika (figure 1), features of the predicted and observed regions of zonal flow now match more closely. The 5^{o} antisunward offset of the center of the model convection electric field results in the zonal flow pattern moving out of the field of view of the radar near local noon. Near local midnight the zonal flow is closest to Chatanika, an invariant latitude of 65^{o}. Poleward of this zonal flow is a region which contains both a discernable antisunward flow component before midnight and a reversed zonal flow in the early morning. The latitudinal extent of the zonal flow pattern and its magnitude as well as the flow characteristics poleward of this zonal flow are well represented by the model predictions. The effects of substorms are not included in the model, thus resulting in its smooth overall appearance when compared to the observed data.

The predictions for the Millstone Hill site also show good general agreement with the data (figure 2). However, the model predictions for Millstone Hill primarily show the main region of zonal flow; only around local midnight is there any evidence of antisunward flow. The magnitude and direction of the predicted and observed flows compare favorably, which is noteworthy since the convection pattern predicted for Millstone Hill is significantly different from that predicted for Chatanika.

Having shown the general agreement between the observations and predictions it is necessary to point out a number of regions of discrepancy between the model and data. The afternoon westward flow is observed at Chatanika between

22-09 UT, whereas this flow is not seen in the predictions until 03 UT. The occurrence of a well defined westward flow region in the early afternoon is a common but not universal feature of Chatanika data.

The west-south-east flow reversal near local midnight occurs in the vicinity of the Harang discontinuity in the ionospheric current pattern. Modelling of the Harang discontinuity requires very localized asymmetric potential distributions (Kamide and Matsushita, 1979), and even then agreement is only obtained in restricted regions. The model used here does not attempt to include the detailed physics associated with the Harang discontinuity. Thus, the general comparison of the observations and predictions in this local time sector is good even though a precise account of the fine structure is not to be expected.

At both Chatanika and Millstone Hill the predicted flow reversal near midnight appears between one and three hours later than observed, and at Chatanika the noon sector pattern is predicted to occur several hours later than seen in the data. There appears to be a systematic time slippage between the predictions of the model and the data.

The model contains a magnetospheric electric field that is symmetric about the noon-midnight meridian. It is mainly this symmetry which determines the local times at which the speed reversal regions are predicted. There are a number of different ways in which the model magnetospheric electric field can be modified to better fit the observed data. Heppner (1977) introduces asymmetries in the two cells, that is, having an enhanced dawn or dusk cell but still maintaining a noon-midnight alignment. Yasuhara et al. (1975) introduce an alignment along a meridian offset by a few hours from the noon-midnight meridian. The direction of the offset on the day side being a few hours before mid-day.

We have examined the relative merits of these two empirical methods of distorting the mapped cross-tail magnetospheric electric field. Adjusting the alignment of the mapped equipotentials so that they are parallel to the 10-22 L.T. direction produced a significant improvement in the agreement between the predicted distribution of the plasma flow vectors and those observed at Chatanika, whereas the other method failed to improve the agreement. Figure 4 shows the predictions of a model identical to that used earlier, except for a skewing of the magnetospheric electric field to give equipotentials parallel to the 10-22 L.T. direction. Better agreement between this model and the Chatanika measurements is seen in the post-noon region. Also the timing of the flow reversals near local noon and midnight is in better agreement with the measurements. This figure is presented as an indication of how empirical adjustments can be used to provide a better match to the data. We are reluctant to recommend the use of this empirical feature at this stage because of the limited data base used in the comparison, and we revert back to the earlier improved model for the following section.

Latitudinal Gradient of Speed Distribution

A second goal of this study was to estimate the latitudinal variation of the flow speed at a given local time. Both Chatanika and Millstone are located such that they see little of the polar cap, but they do provide excellent latitude coverage in the region where the model predicts a latitude gradient in plasma drift speed. The two data sets were averaged over one hour intervals and plotted to show latitudinal gradient of the plasma drift speed. In the model the gradient is the result of a meridionally diminishing potential which varies inversely as the fourth power of sine co-latitude in the magnetic frame (Volland, 1978). The model was also run for an inverse "second power" potential gradient representative of more slowly diminishing potentials, and the

calculated speed gradients were compared directly with the plotted data. Figure 5 shows four of these latitude gradients derived by plotting the logarithm of speed versus geographic latitude. The observations shown are all from Chatanika; the data being represented by points while the solid lines represent the "fourth power" model gradient. In the first panel of figure 5 a dashed line is included; this represents a "second power" model gradient.

It is apparent that the "fourth power" model gradient clearly produces better agreement with the measurements than the "second power" gradient. The four local times shown in figure 5 where chosen for display because a smooth gradient in the speed distribution was clearly evident in the data at these times. A similar comparison between model predictions and observations at other local times indicated that the "fourth power" produced a better agreement than the "second power" for most of the day. However, there were periods during the day when the fall-off of the magnetospheric potential could not be determined unambiguously. For example, in the midnight sector, the boundary between the zonal and the polar cap flows, and the velocity changes across the west-south-east flow reversal region fall within the 72^{o} to 60^{o} region of comparison and a meaningful determination of the slope was not possible.

The comparison of model and observation for Chatanika and Millstone Hill suggest that the magnetospheric electric potential in the fall-off region outside the polar cap is better represented by an "inverse fourth" power than an "inverse second" power. In contrast, Heppner (1977) suggested that the magnetospheric electric potential diminishes more slowly than the fourth power. However, we caution the reader that our conclusion is based on a limited data set. Data taken at other seasons or under other geophysical conditions could produce different results.

4. Summary

The gross features of the diurnal variation of horizontal plasma drift velocities measured concurrently by the incoherent scatter radar installations at Chatanika and Millstone Hill in June, 1978 have been compared with the predictions of a simple model of ionospheric convection. The model used is based on that of Sojka et al. (1979) and refined by offsetting the mapped magnetospheric electric potential 5^{o} from the magnetic pole in the anti-sunward direction. We have shown that the differences in the convection pattern observed at the two sites are consistent with the predictions of this simple model. We are encouraged by the agreement between the model and the data and feel that further comparisons would be fruitful in refining the model. The comparison we have made in this study underlines the importance of taking Universal Time into consideration when analyzing high latitude convection measurements.

ACKNOWLEDGEMENTS

We gratefully acknowledge the help of R. H. Wand in scheduling the Millstone Hill involvement in the collaborative observing program, and in supplying data from the Millstone Hill incoherent scatter radar. We also thank G.S. Stiles for helpful discussions regarding this study and J. Evans for comments on the manuscript. This research was supported by Air Force Contract USAF/ESD F19628-79-C-0025 and NSF grants ATM78-10501 and ATM78-05747 to Utah State University.

REFERENCES

Evans, J. V., W. A. Reed, and P. Stetson, Upgrading the Millstone Hill Radar for International Magnetosphere Studies, Final Report, Lincoln Lab. M.I.T., Lexington, Mass., 1978.

Feldstein, V. I. Some problems concerning the morphology of auroras and magnetic disturbances at high latitudes. Geomagn. Aeron., 3, 183, 1963.

Heppner, J. P. Empirical models of high-latitude electric fields. J. Geophys. Res., 82, 1115-1125, 1977.

Kamide, Y. and S. Matsushita. Simulation studies of ionospheric electric fields and currents in relation to field-aligned currents; 2. Substorms. J. Geophys. Res., in press, 1974.

Meng, C.-I. Diurnal variation of the auroral oval size. J. Geophys. Res., in press, 1979.

Meng, C.-I., R. H. Holzworth and S.-I. Akasofu. Auroral circle-delineating the poleward boundary of the quiet auroral belt. J. Geophys. Res., 82, 164-172, 1977.

Sojka, J. J., W. J. Raitt, and R. W. Schunk. Effect of displaced geomagnetic and geographic poles on high latitude plasma convection and ionospheric depletions. J. Geophys. Res., in press, 1979.

Volland, H. A model of the magnetospheric electric convection field. J. Geophys. Res., 83, 2695-2699, 1978.

Yasuhara, F., Y. Kamide and S.-I. Akasofu. Field-aligned and ionospheric currents. Planet. Space Sci., 23, 1355-1368, 1975.

ILLUSTRATIONS

Fig. 1 Distribution of horizontal plasma drift velocities observed from Chatanika (upper panel) and the predictions for this location of our convection model (lower panel).

Fig. 2 Distribution of horizontal plasma drift velocities observed from Millstone Hill (upper panel) and the predictions for this location of our convection model (lower panel).

Fig. 3 Distribution of horizontal plasma drift velocities predicted for Chatanika by our convection model but with magnetospheric convection mapped symmetrically about the geomagnetic pole.

Fig. 4 Distribution of horizontal plasma drift velocities predicted for Chatanika by our convection model modified to include an empirical skew to the mapped magnetospheric electric field resulting in equipotentials aligned parallel to the 10-22 L.T. direction.

Fig. 5 Variation of plasma drift speeds with geographic latitude for four local time periods as observed at Chatanika (data points). The data were collected over a time period of one hour immediately prior to the time shown. The solid lines are the model predictions for the indicated local times. The dashed line corresponds to the variation in drift speed for an inverse second power decay in the magnetospheric electric potential (see text).

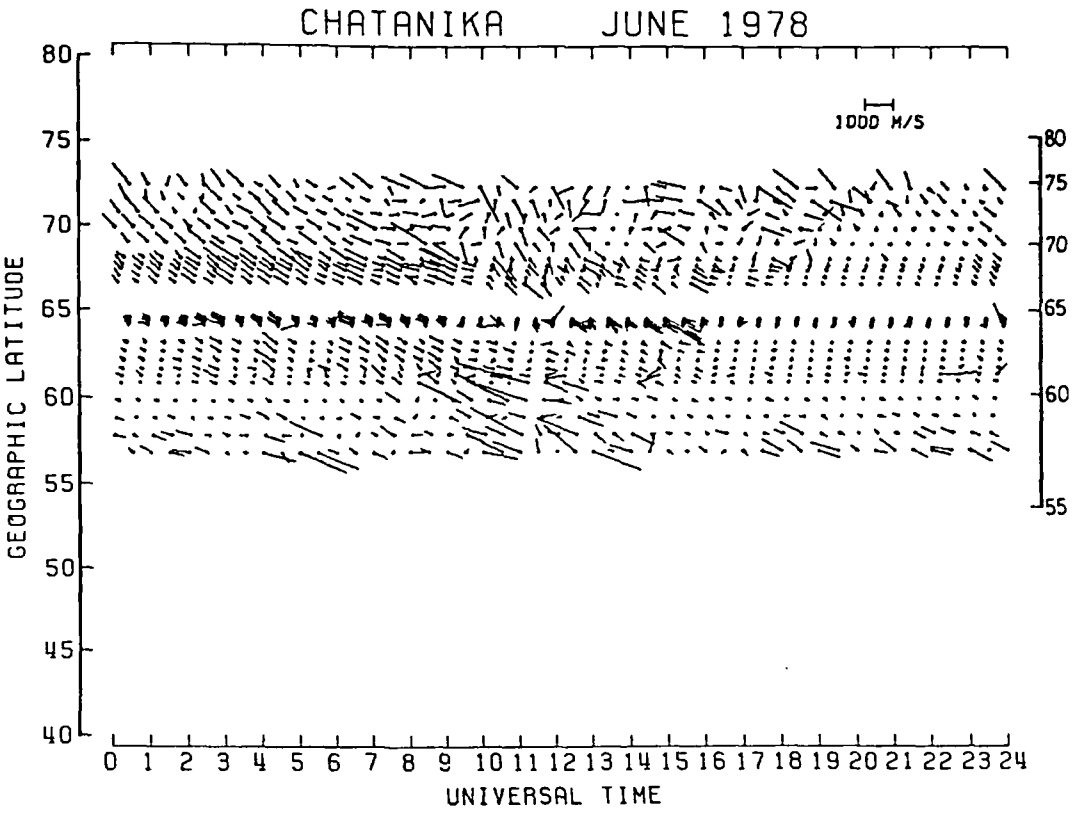
CHATANIKA JUNE 1978
1000 M/S
GEOGRAPHIC LATITUDE
80
75
70
65
60
55
50
45
40
0 1 2 3 4 5 6 7 8 9 10 11 12 13 14 15 16 17 18 19 20 21 22 23 24
UNIVERSAL TIME

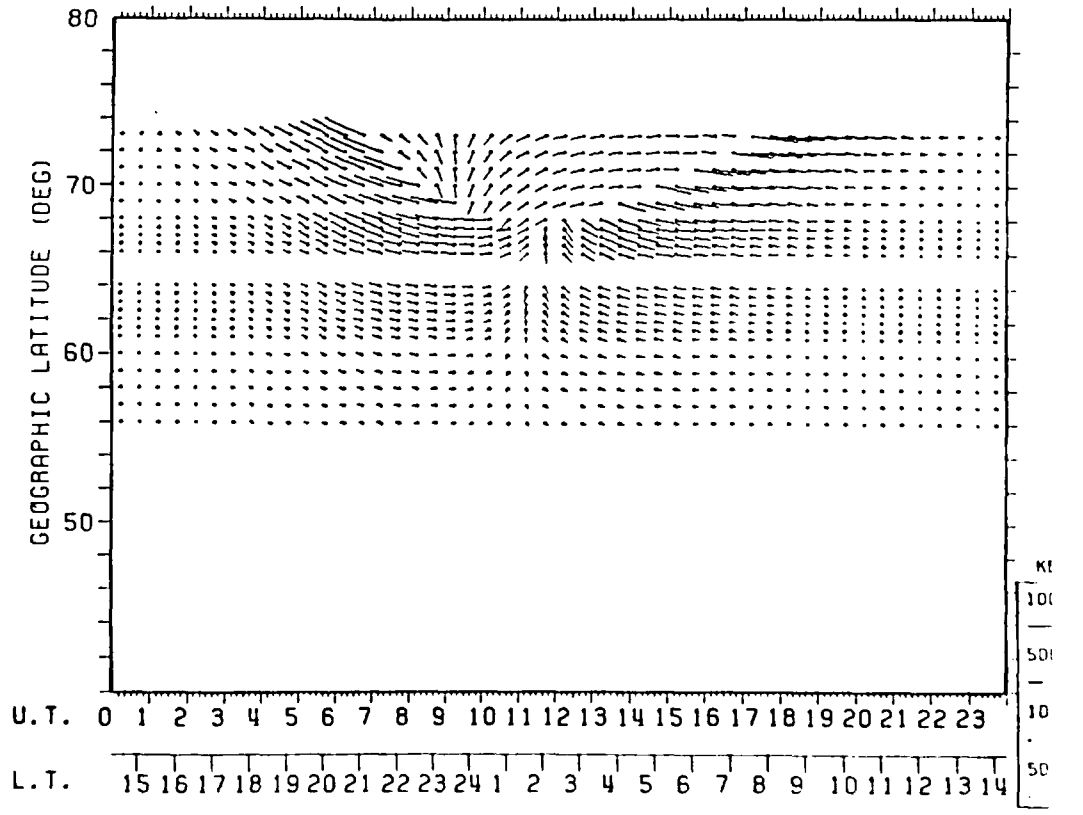
GEOGRAPHIC LATITUDE (DEG)
80
70
60
50
U.T. 0 1 2 3 4 5 6 7 8 9 10 11 12 13 14 15 16 17 18 19 20 21 22 23
L.T. 15 16 17 18 19 20 21 22 23 24 1 2 3 4 5 6 7 8 9 10 11 12 13 14

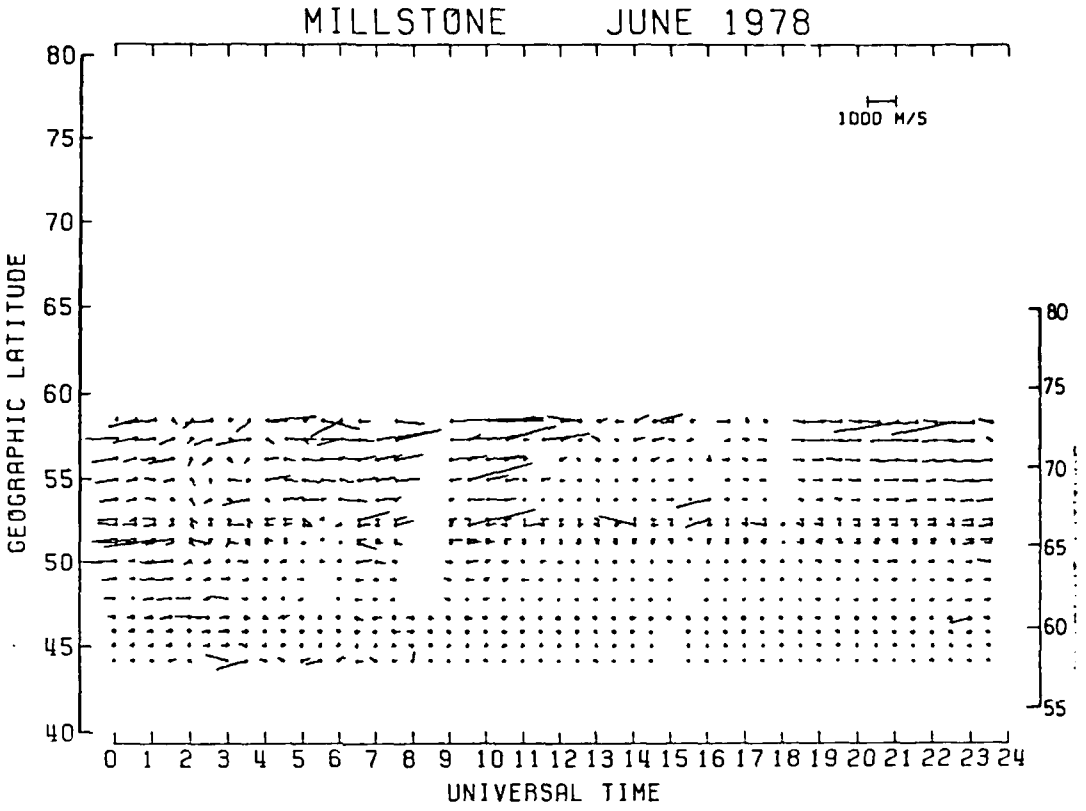
MILLSTONE JUNE 1978
1000 M/S
GEOGRAPHIC LATITUDE
80
75
70
65
60
55
50
45
40
0 1 2 3 4 5 6 7 8 9 10 11 12 13 14 15 16 17 18 19 20 21 22 23 24
UNIVERSAL TIME

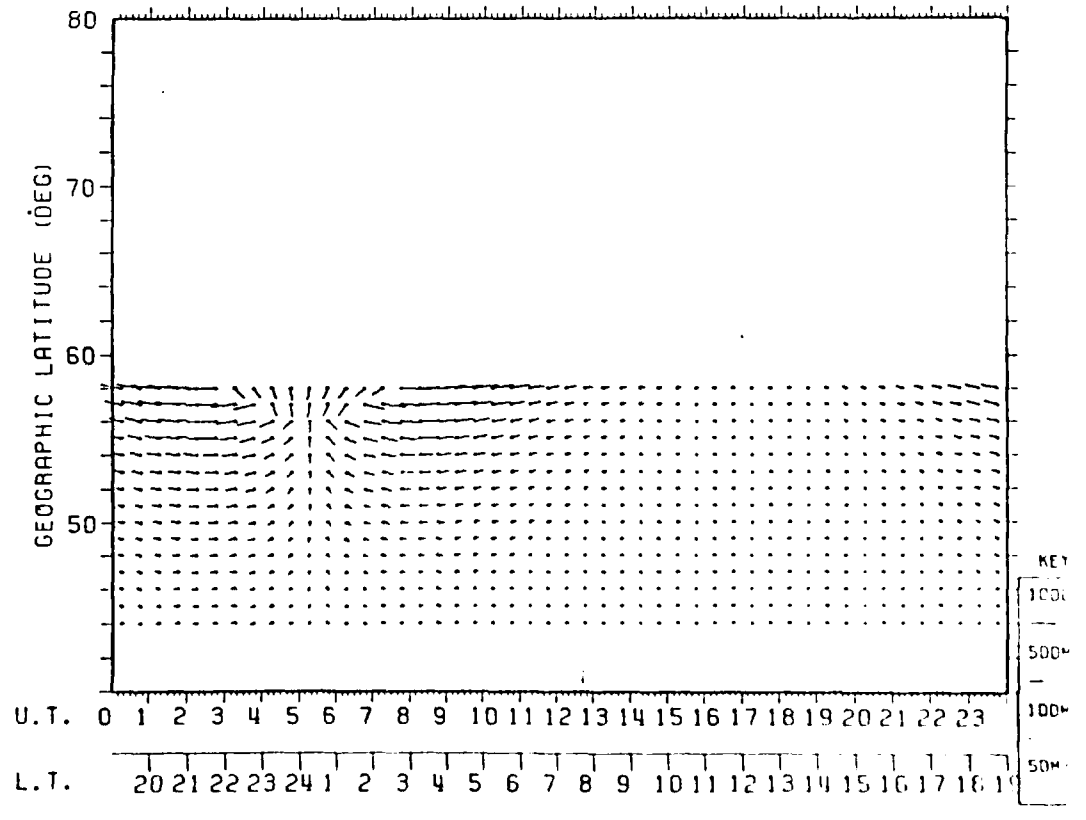
GEOGRAPHIC LATITUDE (DEG)
80
70
60
50
U.T. 0 1 2 3 4 5 6 7 8 9 10 11 12 13 14 15 16 17 18 19 20 21 22 23
L.T. 20 21 22 23 24 1 2 3 4 5 6 7 8 9 10 11 12 13 14 15 16 17 18 19

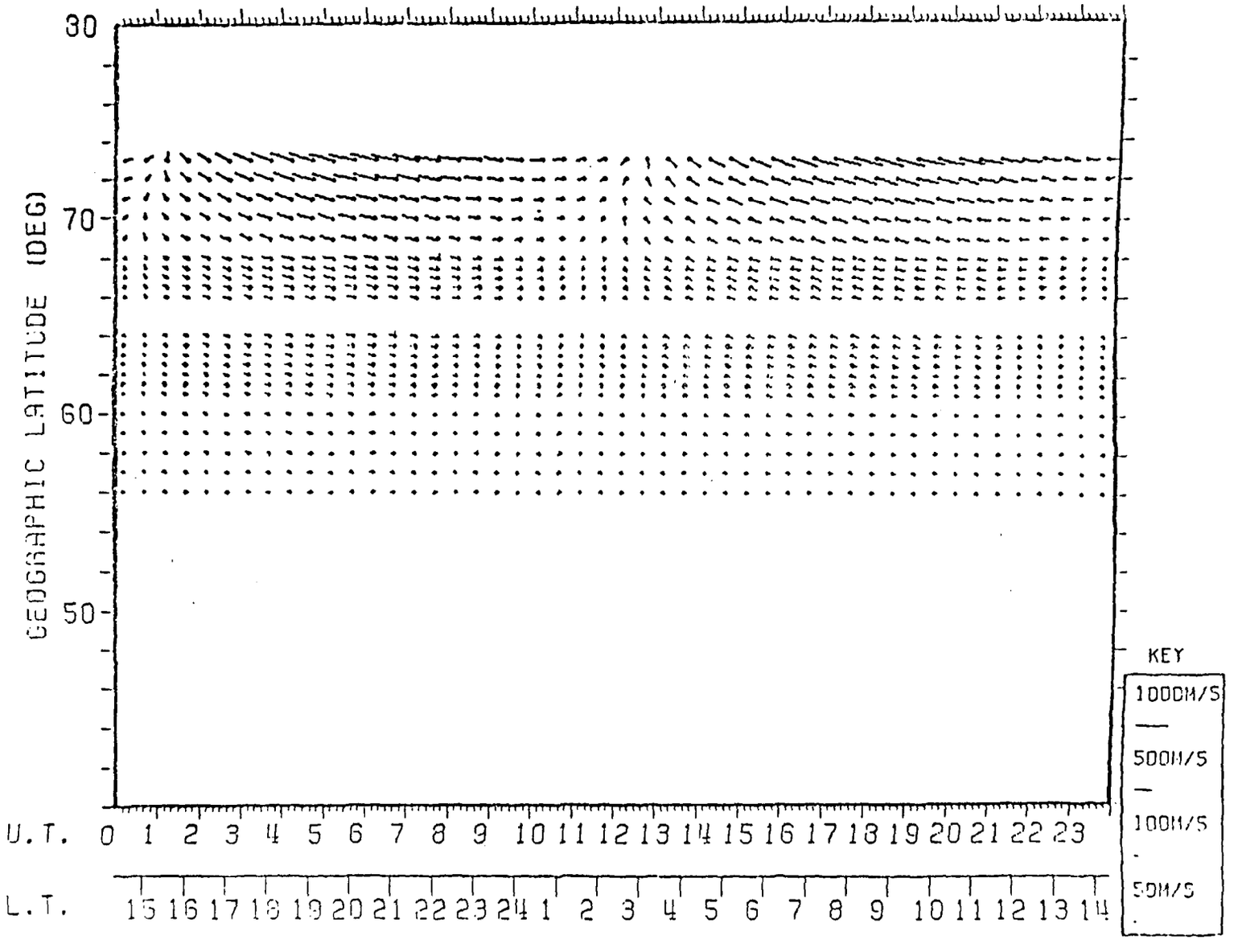
30
70
60
50
GEOGRAPHIC LATITUDE (DEG)
U.T. 0 1 2 3 4 5 6 7 8 9 10 11 12 13 14 15 16 17 18 19 20 21 22 23
L.T. 15 16 17 18 19 20 21 22 23 24 1 2 3 4 5 6 7 8 9 10 11 12 13 14
KEY
1000M/S
500M/S
100M/S
50M/S

Figure 3

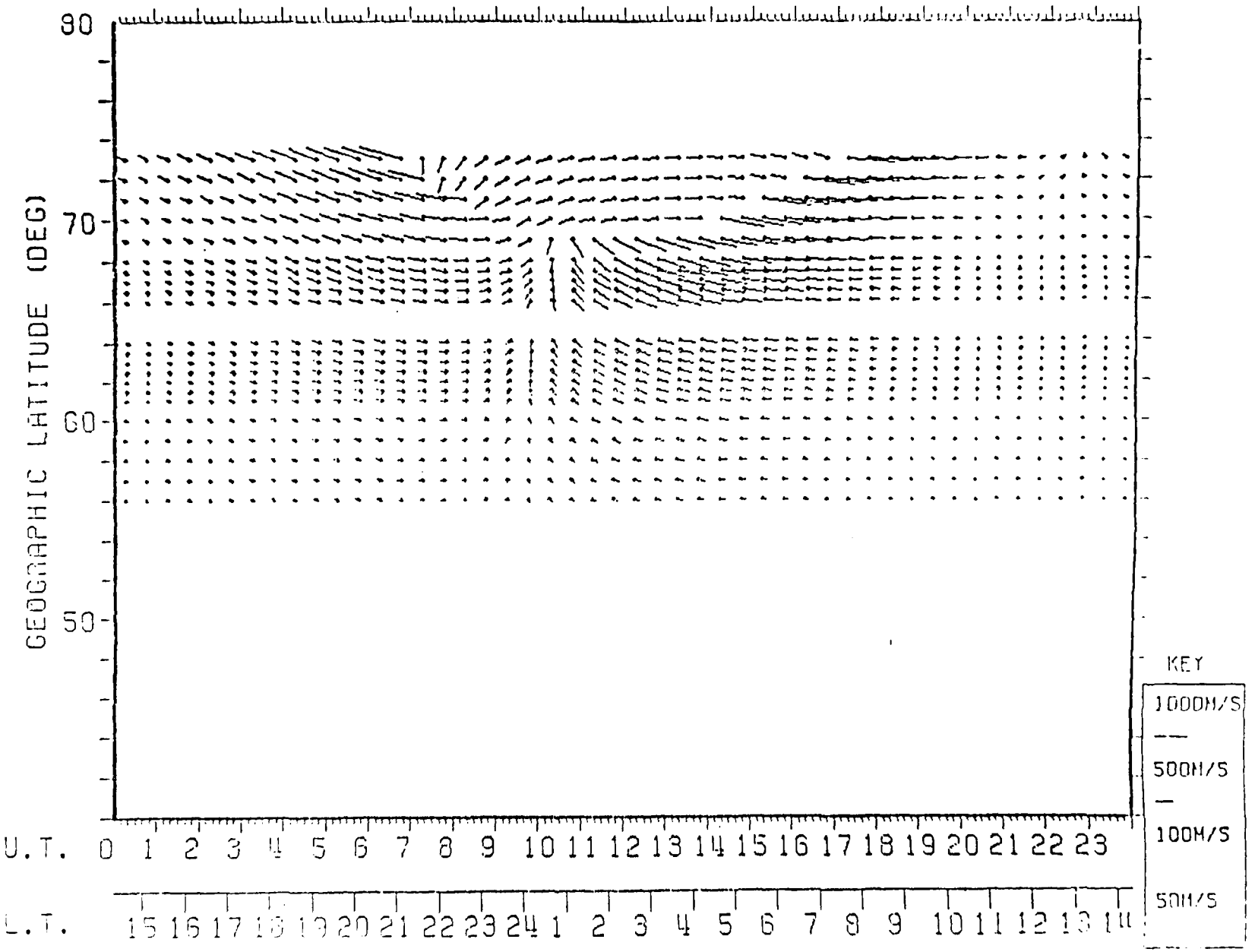
90
70
60
50
GEOGRAPHIC LATITUDE (DEG)
U.T. 0 1 2 3 4 5 6 7 8 9 10 11 12 13 14 15 16 17 18 19 20 21 22 23
L.T. 15 16 17 18 19 20 21 22 23 24 1 2 3 4 5 6 7 8 9 10 11 12 13 14
KEY
1000M/S
500M/S
100M/S
50M/S

Figure 4

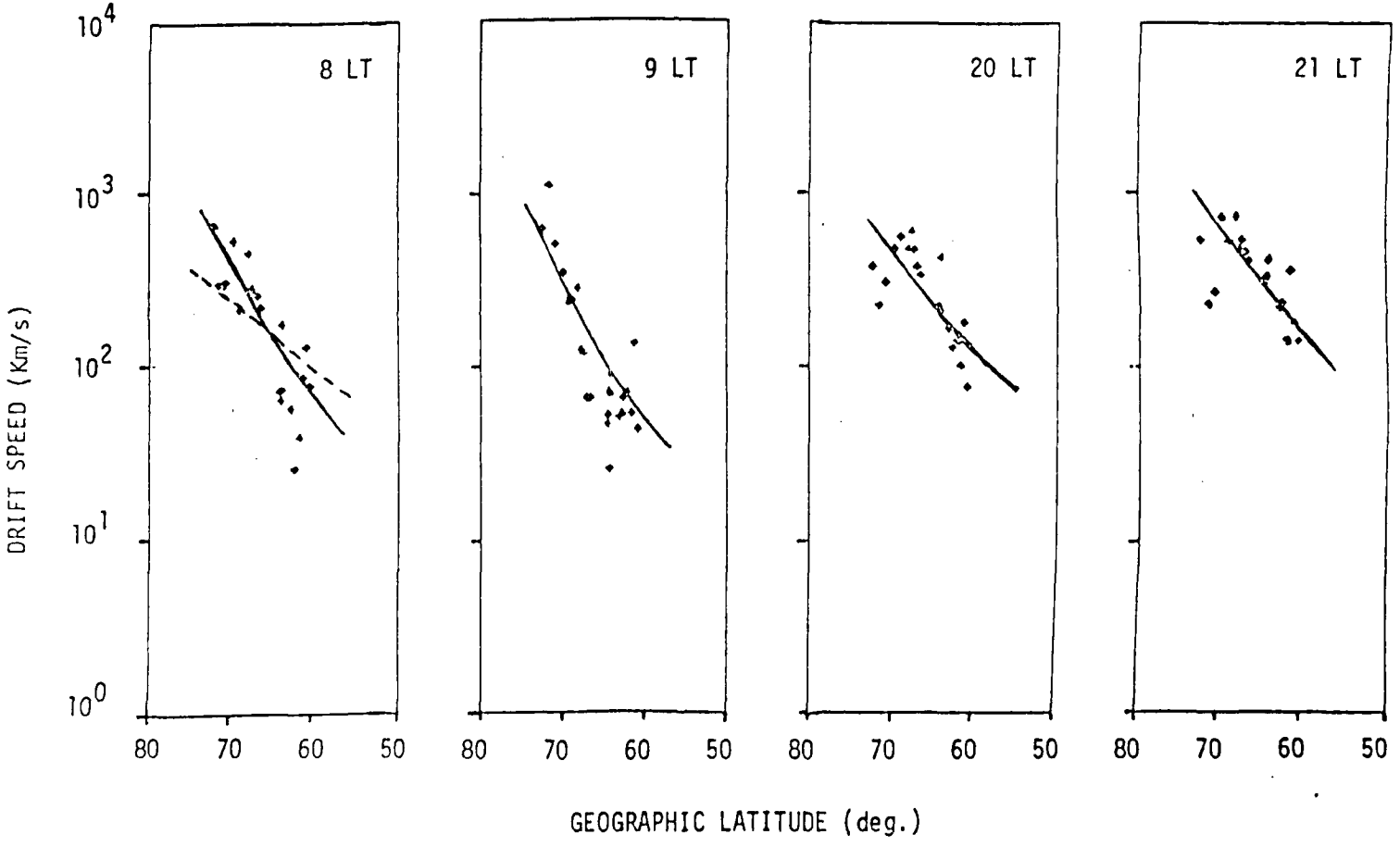
8 LT
9 LT
20 LT
21 LT
DRIFT SPEED (Km/s)
10^4
10^3
10^2
10^1
10^0
80
70
60
50
GEOGRAPHIC LATITUDE (deg.)

Figure 5

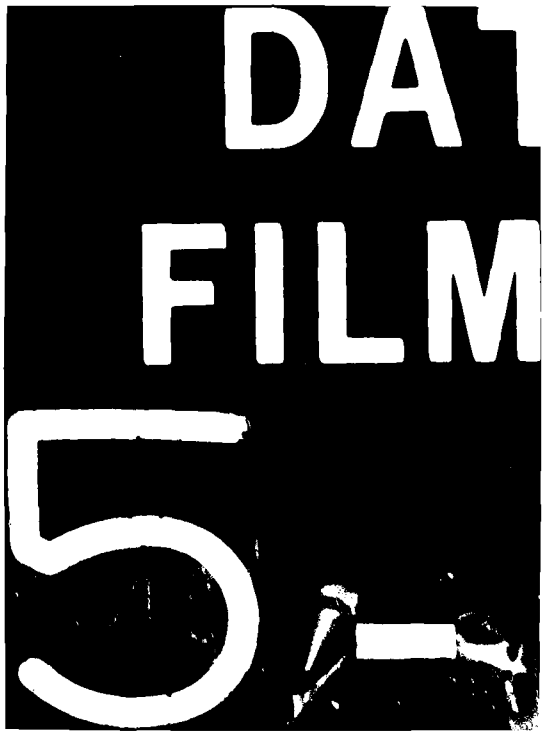
DA
FILM
5